Microscopic Theory of Dipole-Exchange Spin Waves in Ferromagnetic Films: Linear and Nonlinear Processes

R. N. Costa Filho[1,2,*], M. G. Cottam[2], and G. A. Farias[1]

[1] *Departamento de Física, Universidade Federal do Ceará, Campus do Pici, Centro de Ciências, Caixa Postal 6030, 60455-760 Fortaleza, Ceará, Brazil*

[2] *Department of Physics and Astronomy, University of Western Ontario London, Ontario, Canada N6A 3K7*

Abstract

The linear and nonlinear processes in ferromagnetic films at low temperatures ($T \ll T_c$) are studied in a microscopic theory. Both the long-range magnetic dipole-dipole and the Heisenberg exchange interactions to nearest and next-nearest neighbors are included. The results obtained for the linearized spin-wave spectrum are compared with previous macroscopic theories. For ultrathin films (or for large wave vectors) the microscopic theory provides important corrections. The nonlinear dynamics of the spin waves are studied through a finite-temperature perturbation theory based on Feynman diagrams. We obtain explicit results for the energy shift and damping (or reciprocal lifetime) of the dipole-exchange spin waves due to all possible three-magnon and four-magnon processes involving combinations of the surface and quantized bulk spin waves at low temperatures. To investigate different dipole interaction strengths (relative to the exchange) numerical results are presented using parameters for Fe, EuO, and $GdCl_3$.

75.70.Ak, 75.30.Ds, 76.50.+g

I. INTRODUCTION

Ultrathin ferromagnetic films are of great interest due to their widespread technological applicability.[1] This is because these films can have properties, both static and dynamic, that differ significantly from bulk samples of the same material. For example, it is well known theoretically that, in these quasi-two-dimensional systems, the short-range exchange interactions alone are not sufficient to establish a ferromagnetically ordered ground state,[2,3] and it is necessary to take into account the anisotropy and long-range character of the dipolar interactions. Regarding the spin dynamics in ferromagnetic films, a macroscopic (or continuous medium) theory for the dipole-dominated regime was given by Damon and Eshbach[4] in terms of magnetostatic modes. They identified a surface branch to the spectrum, now known as the Damon-Eshbach (DE) mode. Subsequently there has been extensive work to generalize the magnetostatic theory to include also the exchange effects, leading to dipole-exchange theory (for reviews see, e.g., Refs. 5-7). In these theories the DE surface mode becomes modified and various quantization effects become evident for the bulk modes. In addition, Benson and Mills[8] considered a microscopic formalism for the dipole interactions in a thin ferromagnetic film, obtaining a rapidly converging series for the dipole sums. More recently, their approach has been extended to a description of the dipole-exchange spin waves (SW) in various ferromagnetic and antiferromagnetic films.[9–11]

All of the studies mentioned above neglected the higher-order effects that give rise to SW interactions. These occur because the SW are not exact eigenstates of the magnetic Hamiltonian and they are the source of several nonlinear effects,[6,7] such as parallel pumping of SW, auto-oscillations and the transition to chaos, soliton formation, and energy renormalization and damping of the SW modes. Previous studies of the SW interactions *in films* were carried out from a macroscopic point of view,[5–7] where the dipolar terms were introduced using Maxwell's equations. Again, this should be appropriate for small wave vectors and for moderate film thickness.

In infinite ferromagnets, either with or without the inclusion of the dipolar interactions,

the treatment of the interactions between the bulk SW modes is well established.[12] The dominant contributions at $T \ll T_c$ come from three-magnon confluence and splitting processes and from four-magnon scattering processes. In the special case of a Heisenberg ferromagnet, where there are only exchange interactions, the three-magnon process is absent. However, for a finite ferromagnet, the presence of surfaces leads to a richer SW spectrum that may consist of one or more localized surface SW modes as well as the bulk modes (which become quantized in a film geometry). The occurrence of surface and modified bulk modes in a finite ferromagnet will give rise to more complicated schemes or SW interactions, since the scattering processes may now involve both types of modes.

There has previously been a number of calculations for SW interactions in semi-infinite *Heisenberg* ferromagnets at low temperatures $T \ll T_c$ using a Hamiltonian approach. In particular, results for the damping and the energy renormalization of the surface SW were obtained in some special cases by Tarasenko and Kharitonov[13] and Mazur and Mills.[14] More detailed results, which were applicable to both surface and bulk (volume SWs and induced pinning through surface anisotropy and modified surface exchange, were derived by Kontos and Cottam[15,16] using a diagrammatic perturbation method.

In the above-mentioned studies for Heisenberg systems, the dipole-dipole interactions were ignored, leading to a description of SW interactions at $T \ll T_c$ only in terms of the leading-order four-magnon processes. When the dipolar terms are included there are also three-magnon processes involving the splitting of SW into two SW modes and the confluence of two SW modes into a single SW. For example, Rahman and Mills[17] calculated the renormalized energies for the bulk and Damon-Eshbach surface SW in the dipolar-exchange regime. For ferromagnetic films in this regime of long wavelengths (or small wave vectors), there have been extensive calculations of the nonlinear SW properties using a macroscopic (or continuous-medium) type of theory.[6,7,17,18] A nonlinear *microscopic* theory, based on a Hamiltonian approach, allows us to study the SW interactions and the renormalization of the discrete SW modes.

The aim of this paper is to provide a *microscopic* theory to calculate linear and nonlinear

properties of the localized surface SW and the quantized bulk SW in ferromagnetic films. This is done for all wave-vector values and for any film thickness. The theory includes the effects of the short-range exchange coupling and the long-range dipole-dipole interactions between spins. The latter interactions are evaluated in a similar manner to recent work for ferromagnetic and antiferromagnetic films in the *linear* SW regime.[9–11] We obtain the dependence of the SW energies (for each of the discrete branches) on the number of layers of the film, the variation of the exchange parameters (including nearest and next-nearest neighbors), the strength of the dipolar interaction, and the in-plane wave vector. We also develop a perturbation formalism to study the linear and leading-order nonlinear SW processes of in ferromagnetic thin films at low temperature $T \ll T_C$. We use a Hamiltonian formalism to find formal expressions for the SW interaction terms involving products of three and four boson operators, representing the three- and four-magnon processes respectively. The method basically involves diagonalizing the non-interacting part of the Hamiltonian that is bilinear in the boson operators by making a transformation to a new set of boson operators, and then using it to define "unperturbed" Green functions. The perturbation terms, involving either three or four boson operators, are each transformed to the new boson operators and used to define interaction vertices within a Feynman diagram formalism.

This paper is arranged as follows. Section II describes the Hamiltonian with exchange, Zeeman, and dipolar terms, as well as the assumed geometry of the ferromagnetic film. The method basically involves generalizing some previous calculations for nonlinear SW processes in semi-infinite Heisenberg ferromagnets[15] to include the dipolar interactions and the effect of finite film thickness. The transformations of the dipole sums that enter into our Hamiltonian were calculated according to the method described in Ref. 8. Results for the linear (noninteracting) SW spectrum of the film are derived in Sec. III, where we include numerical applications to different materials. In Sec. IV we analyze the higher order terms in the Hamiltonian that lead to SW interactions. At low temperatures $T \ll T_c$, it is shown that the dominant interaction processes involve three- and four- magnon scattering, by analogy with infinite ferromagnets.[12]. In Sec. V we introduce the Green function formalism,

associated with the diagonalized Hamiltonian $H^{(2)}$ of the system, and employ it to obtain general expressions for the energy shift and damping of the magnons in a ferromagnetic film in terms of a SW self-energy contribution. A diagrammatic perturbation technique is then employed in Sec. VI to calculate the SW self-energy due to the three- and four-magnon processes. In Sec. VII we discuss the numerical results applied to three different materials: Fe, where the ratio of dipolar to exchange strengths is very small; $GdCl_3$, where the dipolar terms are relatively strong; and EuO, which represents an intermediate case. The overall conclusions are in Sec. VIII, while some of the mathematical expressions are quoted in the Appendices.

II. HAMILTONIAN AND FILM GEOMETRY

We consider a ferromagnetic film with N atomic layers of spins (with quantum number S) arranged on a simple cubic lattice with lattice constant a. The external magnetic field H_0 and the static magnetization M are assumed to be parallel to z direction, the surface of the film is in the $x-z$ plane, while the y-axis is perpendicular to the surface. We can generalize to the other crystal structures, surface orientations, and magnetization directions in a straightforward manner.

The system will be represented by the Hamiltonian

$$H = -\frac{1}{2}\sum_{ij} J_{ij}\mathbf{S}_i \cdot \mathbf{S}_j - g\mu_B H_0 \sum_i S_i^z + \frac{1}{2}(g\mu_B)^2 \sum_{ij} D_{ij}^{\alpha\beta} S_i^\alpha S_j^\beta \tag{1}$$

where $\mathbf{S}_i$ is the spin at site i, and J_{ij} is the exchange coupling between sites labeled i and j. It is assumed that the exchange coupling is J_1 and J_2 for nearest and next-nearest neighbors respectively, and zero otherwise. The second term of Eq. (1) describes the Zeeman interaction of the spins with an externally applied field H_0. The dipole-dipole interaction between spins in different lattice sites is represented by the last term in Eq. (1), where α and β denote components x, y, or z, and

$$D_{ij}^{\alpha\beta} = \left\{ \frac{|\mathbf{r}_{ij}|^2\delta_{\alpha\beta} - 3r_{ij}^\alpha r_{ij}^\beta}{|\mathbf{r}_{ij}|^5} \right\} \tag{2}$$

where $\mathbf{r}_{ij} = \mathbf{r}_j - \mathbf{r}_i$, and the case $i = j$ is excluded from the sums in Eq. (1). Here we consider, for simplicity, that the exchange constants do not change near the surface of the film, and surface anisotropy fields are also neglected. However, we can easily include these changes in our calculations.

The Hamiltonian may be written in terms of boson operators using the Holstein-Primakoff transformation,[12] and can be expanded as $H = H^{(2)} + H^{(3)} + H^{(4)} + \ldots$ (apart from a constant), where $H^{(m)}$ denotes the term involving a product of m boson operators. The non-interacting (linear) SW modes are described by the quadratic term $H^{(2)}$ that has the following form

$$H^{(2)} = \sum_{\mathbf{q}nn'} \left\{ A^{(2)}_{nn'}(\mathbf{q}) a^\dagger_{\mathbf{q}n} a_{\mathbf{q}n'} + B^{(2)}_{nn'}(\mathbf{q}) [a_{\mathbf{q}n} a_{-\mathbf{q}n'} + a^\dagger_{\mathbf{q}n} a^\dagger_{-\mathbf{q}n'}] \right\}. \tag{3}$$

Here we are using a representation of the boson operators $a^\dagger$ and a in terms of a 2D wave vector $\mathbf{q} = (q_x, q_z)$ parallel to the film surfaces and indices n and $n'(= 1, 2, \ldots, N)$ that label the atomic layers parallel to the surface. The amplitude factors are

$$\begin{aligned} A^{(2)}_{nn'}(\mathbf{q}) = & \left\{ g\mu_B H_0 + S \left[u_n(0) - u_n(\mathbf{q}) + v_{n,n+1}(0) + v_{n,n-1}(0) - (g\mu_B)^2 \sum_{n''} D^{zz}_{nn''}(0) \right] \right\} \delta_{nn'} \\ & - S[v_{n,n+1}(\mathbf{q}) \delta_{n',n+1} + v_{n,n-1}(\mathbf{q}) \delta_{n',n-1} + (g\mu_B)^2 D^{zz}_{nn'}(\mathbf{q})], \end{aligned} \tag{4}$$

$$B^{(2)}_{nn'}(q) = \frac{1}{4} S (g\mu_B)^2 \left[D^{xx}_{nn'}(\mathbf{q}) - D^{yy}_{nn'}(\mathbf{q}) - 2i D^{xy}_{nn'}(\mathbf{q}) \right]. \tag{5}$$

Here we have introduced

$$u_n(\mathbf{q}) = 2J_1 \sigma_1(\mathbf{q}) + 4J_2 \sigma_2(\mathbf{q}) \tag{6}$$

and

$$v_{n,n\pm1}(\mathbf{q}) = J_1 + 2J_2 \sigma_1(\mathbf{q}) \tag{7}$$

as intra-layer and adjacent-layer Fourier transforms of the exchange interactions, with $\sigma_1(\mathbf{q}) = [\cos(q_x a) + \cos(q_z a)]$ and $\sigma_2(\mathbf{q}) = \cos(q_x a) \cos(q_z a)$. The quantities $D^{\alpha\beta}_{nn'}$ are analogous Fourier transforms with respect to $\mathbf{q}$ of the dipole interactions defined in Eq. (2). The expressions for these terms are given in Appendix A.

In the next section we discuss the linearized SW spectrum, which is obtained using $H^{(2)}$, before proceeding in Sec. IV to a description of the nonlinearities produced by the higher-order terms.

III. LINEARIZED SW SPECTRUM

In the linear approximation the SW spectrum is obtained by applying the standard equation of motion $i\hbar dA/dt = [A, H]$ (for any operator A) to the boson operators $a^\dagger_{\mathbf{q}n}$ and $a_{\mathbf{q}n}$ in layer n, with the Hamiltonian H replaced by $H^{(2)}$. Taking $\hbar = 1$ and assuming a time dependence for the modes like $\exp(-i\omega t)$, we obtain the sets of equations

$$\omega a^\dagger_{\mathbf{q}n} = \sum_{n'} \left\{ A^{(2)}_{nn'}(\mathbf{q}) a^\dagger_{\mathbf{q}n} + [B^{(2)}_{nn'}(\mathbf{q}) + B^{(2)}_{n'n}(-\mathbf{q})] a_{-\mathbf{q}n'} \right\}, \tag{8}$$

$$-\omega a_{-\mathbf{q}n'} = \sum_{n'} \left\{ [B^{(2)}_{nn'}(-\mathbf{q}) + B^{(2)}_{n'n}(\mathbf{q})] a^\dagger_{\mathbf{q}n} + A^{(2)}_{nn'}(-\mathbf{q}) a_{-\mathbf{q}n'} \right\}. \tag{9}$$

There are $2N$ coupled equations altogether, where N is the number of layers of the film. Using the symmetry properties $A^{(2)}_{nn'}(\mathbf{q}) = A^{(2)}_{nn'}(-\mathbf{q})$ and $B^{(2)}_{n'n}(-\mathbf{q}) = B^{(2)}_{nn'}(\mathbf{q})$, which arise from the properties of the dipole sums (see Appendix A) and the property $J_{ij} = J_{ji}$, the condition for there to be non-trivial solutions of Eqs. (8) and (9) can be expressed as

$$\det \begin{bmatrix} \mathbf{A}^{(2)}(\mathbf{q}) - \omega \mathbf{I}_N & 2\tilde{\mathbf{B}}^{(2)}(\mathbf{q}) \\ 2\mathbf{B}^{(2)}(\mathbf{q}) & \mathbf{A}^{(2)}(\mathbf{q}) + \omega \mathbf{I}_N \end{bmatrix} = 0. \tag{10}$$

Here $\mathbf{A}^{(2)}(\mathbf{q})$ and $\mathbf{B}^{(2)}(\mathbf{q})$ are $N \times N$ matrices with elements defined in Eqs. (4) and (5) respectively, and $\mathbf{I}_N$ is the $N \times N$ unit matrix. The discrete SW frequencies in the film correspond to the N solutions for positive ω of Eq. (10). They are degenerate in magnitude with the negative-frequency solutions.

Numerical applications of the above theory have been made using parameters appropriate to thin films of the ferromagnets $GdCl_3$ ($T_c \approx 2.2$ K) and EuO ($T_c \approx 69$ K). These are chosen as representing different strengths of the dipole interactions relative to the exchange interactions. They correspond, in fact, to increasing exchange strengths, as can be inferred

from the increasing T_c values. In general, the dipolar interactions will have their most significant effect on the long-wavelength (small $\mathbf{q}$) SW properties in each material, while the exchange effects dominate at shorter wavelengths. We note that thin-film samples of EuO have been employed in SW experiments, e.g., using Brillouin light scattering and microwave resonance techniques.[19,20] Consequently, their magnetic parameters are fairly well known. In the case of $GdCl_3$ the approximate parameters can be deduced from a study of the SW spectrum in bulk samples (e.g., see Ref. 21). The ratio of $4\pi M$ (which characterizes the dipolar strength) to the bulk exchange field H_{Ex} is approximately 1.5 for $GdCl_3$ and 0.063 for EuO.

It is well known that, in Heisenberg ferromagnetic films, exchange-dependent surface SW modes may occur[5,7] that have properties quite different from the Damon-Eshbach (DE) surface mode[4,5] of the magnetostatic theory. They occur, for example, if the exchange coupling between spins in the surface layers is modified or if effects of next-nearest neighbor exchange interactions are included. Here we study such exchange surface modes (as well as the DE type of surface modes) by including the next-neighbor exchange interactions J_2 in our numerical calculations for ultrathin films.

We first show calculations for a 16-layer EuO film, taking $4\pi M = 2.4$ T, $H_{Ex} = 38$ T, and $H_0 = 0.36$ T. Note that the bulk exchange field is given by $g\mu_B H_{Ex} = 6S(J_1 + 2J_2)$ for the model simple-cubic structure. Here J_1 and J_2 are effective exchange parameters because EuO normally has a fcc structure. In Fig. 1 plots are shown for the frequency in GHz (converted using $\gamma = 28$ GHz/T) of the lowest few discrete SW branches versus the ratio J_2/J_1 and versus $q_x a/\pi$ (which ranges from 0 at the Brillouin zone center to 1 at the zone boundary) for small q_x. We have taken the case of $q_z = 0$ (the Voigt geometry), for which it is known that there is a Damon-Eshbach (DE) surface mode[4] in the magnetostatic continuum limit where exchange is neglected. In Fig. 1(a) the dependence of the two lowest branches of the SW dispersion relation on J_2/J_1 is shown for two different values of $q_x a/\pi$. For $q_x \approx 0$ we note that the first branch has almost no dependence on J_2/J_1. That is expected since this lowest branch is essentially the DE mode. The second branch has a smooth dependence

on J_2. For $q_x = 0.01$ both modes increase their energy as J_2/J_1 increases. These effects are more noticeable in Fig. 1(b), where a plot of the frequency against the wave vector is shown for three different values of J_2/J_1. The purely magnetostatic DE mode would tend to the approximate limiting value of 43 GHz with increasing q_x. While it can be seen in both cases that there is a relatively flat (dispersionless) branch near this frequency, the upward curvature apparent at larger q_x is due to the exchange terms. In the region near 35 GHz for small $q_x a/\pi$ where two branches (the lowest bulk mode and the analog of the DE mode) come close together, but do not cross. This phenomenon of a near "crossover", with mode repulsion, signifies a strong mixing (or hybridization) of two modes.

In Fig. 2 we show the behavior of the lowest four SW branches for very small wave vectors in a $GdCl_3$ film with $N = 16$, considering $J_2/J_1 = 0$ (dashed lines) and $J_2/J_1 = 0.25$ (solid lines). This shows the effects of the next-nearest neighbor exchange. For this material, we use the parameters $4\pi M = 0.82$ T, $H_{Ex} = 0.54$ T, and $H_0 = 0.36$ T. It can be seen that a purely magnetostatic DE mode starts at $q_x = 0$ at the frequency 18.25 GHz in both cases. By contrast with the same film thickness for EuO in Fig. 1, we can see that the DE mode in the $GdCl_3$ case affects several of the bulk modes of the spectrum, which is a consequence of the larger $4\pi M/H_{Ex}$ in this material compared with EuO.

In the numerical examples shown above, the limiting frequency of the DE mode (as $q_x \to 0$) is very close to the value $[H_0(H_0 + 4\pi M)]^{1/2}$ predicted by the macroscopic magnetostatic theory[4] in the Voigt geometry. On the other hand, the magnetostatic theory predicts that the DE branch becomes flat, tending to a limiting value of $H_0 + 2\pi M$ when q_x is large compared with the reciprocal of the film thickness. This behavior is followed approximately in our theory, but there is an additional upward curvature to all SW branches due to exchange. This is in addition to the hybridization effects and the microscopic corrections to continuum dipole-exchange theories.

IV. HIGHER ORDERS: SW INTERACTIONS

The higher order terms in the expansion of the Hamiltonian, i.e., the terms $H^{(m)}$ with $m \geq 3$, correspond to the nonlinear aspects of the SW dynamics including interactions between the SW modes. As in the case of bulk (effectively infinite) ferromagnets,[12] the leading-order effects for $T \ll T_C$ come from the terms that have three and four boson operators ($H^{(3)}$ and $H^{(4)}$).

The term $H^{(3)}$ depends only on the dipolar interactions and has the form:

$$H^{(3)} = \frac{1}{2} \sum_{\mathbf{k}\mathbf{q}nn'} A^{(3)}_{nn'}(\mathbf{k}) \left[a^\dagger_{\mathbf{k}n'} a^\dagger_{\mathbf{q}-\mathbf{k}n} a_{\mathbf{q}n} + a^\dagger_{\mathbf{q}n} a_{\mathbf{q}-\mathbf{k}n} a_{\mathbf{k}n'} \right], \tag{11}$$

with the amplitude term given by

$$A^{(3)}_{nn'}(\mathbf{k}) = \sqrt{2S} g^2 \mu_B^2 \left[D^{xz}_{nn'}(\mathbf{k}) - i D^{yz}_{nn'}(\mathbf{k}) \right]. \tag{12}$$

This represents the splitting and confluence processes inherent in the three-magnon processes.

By contrast, the four-magnon interaction $H^{(4)}$ has parts involving both dipolar and exchange terms:

$$\begin{aligned} H^{(4)} = \frac{1}{2} \sum_{\mathbf{k}\mathbf{k}'\mathbf{q}nn'} \Big\{ & A^{(4)}_{nn'}(\mathbf{k}) a^\dagger_{\mathbf{k}'n} a^\dagger_{\mathbf{q}-\mathbf{k}'n} a_{\mathbf{q}-\mathbf{k}n} a_{\mathbf{k}n'} + A^{(4)}_{nn'}(-\mathbf{k}') a^\dagger_{\mathbf{k}'n'} a^\dagger_{\mathbf{q}-\mathbf{k}'n} a_{\mathbf{q}-\mathbf{k}n} a_{\mathbf{k}n} \\ & -2B^{(4)}_{nn'}(\mathbf{k}-\mathbf{k}') a^\dagger_{\mathbf{k}'n'} a^\dagger_{\mathbf{q}-\mathbf{k}'n} a_{\mathbf{q}-\mathbf{k}n} a_{\mathbf{k}n'} + C^{(4)}_{nn'}(\mathbf{k}) [a^\dagger_{\mathbf{q}n} a_{\mathbf{q}-\mathbf{k}-\mathbf{k}'n} a_{\mathbf{k}'n} a_{\mathbf{k}n'} + h.c] \Big\}. \end{aligned} \tag{13}$$

In this case the amplitude coefficients are defined by

$$A^{(4)}_{nn'}(\mathbf{q}) = \frac{1}{2} \left[u_n(\mathbf{q}) \delta_{nn'} + v_{n,n+1}(\mathbf{q}) \delta_{n',n+1} + v_{n',n-1}(\mathbf{q}) \delta_{n',n+1} + \frac{1}{2} (g\mu_B)^2 D^{zz}_{nn'}(\mathbf{q}) \right], \tag{14}$$

$$B^{(4)}_{nn'}(\mathbf{q}) = A^{(4)}_{nn'}(\mathbf{q}) - \frac{3}{4} (g\mu_B)^2 D^{zz}_{nn'}(\mathbf{q}), \tag{15}$$

$$C^{(4)}_{nn'}(\mathbf{q}) = -(1/S) B^{(2)}_{nn'}(\mathbf{q}). \tag{16}$$

This interaction represents the scattering of a pair of magnons into another pair of magnons.

We note that each term in Eqs. (11) and (13) conserve the 2D in-plane wave vector, since there is translational symmetry in the $x-z$ plane. The dependence in the y-direction is taken into account the the summations over layer indices n and n'. The above $H^{(3)}$ and $H^{(4)}$ interactions are the analogs (in a microscopic theory) of the expressions used in macroscopic theories to describe a wide range on nonlinear effects,[5,6] as mentioned earlier. For example, they describe processes whereby energy from a given SW (with, say, wave vector $\mathbf{q}$ and from the discrete branch ν) can be transferred to other SW modes of the film. Thus they can be used to calculate the damping (or reciprocal lifetime) of any given SW, as well as the shift (or renormalization) in its energy. This can be accomplished using a diagrammatic perturbation method with Green functions.

V. THE GREEN FUNCTION FORMALISM

We establish a Green function formalism for the film geometry with N atomic layers parallel to the surfaces. The method is analogous to that used in previous diagrammatic perturbation calculations for the effects of SW interactions in semi-infinite Heisenberg ferromagnets,[15,16] but generalized here to include the dipolar terms and the quantization of the modes due to finite film thickness.

The starting point to the diagrammatic formalism is the expansion of the Hamiltonian into terms containing products of two, three, and four boson operators. The relevant expressions for these terms are given in Eqs. (3), (11), and (13). The bilinear term $H^{(2)}$, which we shall treat as the non-interacting part of the Hamiltonian, can first be rewritten as

$$H^{(2)} = -\frac{1}{2}\sum_{\mathbf{q}} \mathrm{Tr}\left[\mathbf{A}^{(2)}(\mathbf{q})\right] + \frac{1}{2}\sum_{\mathbf{q}} \tilde{\mathcal{A}}^{\dagger}_{\mathbf{q}}\, \mathcal{X}(\mathbf{q})\, \mathcal{A}_{\mathbf{q}}, \tag{17}$$

where

$$\mathcal{X}(\mathbf{q}) = \begin{pmatrix} \tilde{\mathbf{A}}^{(2)}(\mathbf{q}) & 2\tilde{\mathbf{C}}^{(2)}(\mathbf{q}) \\ 2\tilde{\mathbf{B}}^{(2)}(-\mathbf{q}) & \mathbf{A}^{(2)}(-\mathbf{q}) \end{pmatrix}. \tag{18}$$

Here we have defined operators $\mathcal{A}^{\dagger}_{\mathbf{q}}$ and $\mathcal{A}_{\mathbf{q}}$ that create and destroy wave vector $\mathbf{q}$ by

$$\mathcal{A}_{\mathbf{q}}^{\dagger} = \begin{pmatrix} \mathbf{a}_{\mathbf{q}}^{\dagger} \\ \mathbf{a}_{-\mathbf{q}} \end{pmatrix} \quad , \quad \mathcal{A}_{\mathbf{q}} = \begin{pmatrix} \mathbf{a}_{\mathbf{q}} \\ \mathbf{a}_{-\mathbf{q}}^{\dagger} \end{pmatrix}, \tag{19}$$

respectively, where $a_{\mathbf{q}}^{\dagger}$ and $a_{\mathbf{q}}$ are N-component column matrices whose nth elements are $a_{\mathbf{q},n}^{\dagger}$ and $a_{\mathbf{q},n}$. The tilde denotes a matrix transpose, and $\mathbf{A}^{(2)}(\mathbf{q})$ and $\mathbf{B}^{(2)}(\mathbf{q})$ are the $N \times N$ matrices with elements given by $A_{nn'}^{(2)}(\mathbf{q})$ and $B_{nn'}^{(2)}(\mathbf{q})$ defined in Eqs. (4) and (5).

The first term in Eq. (17) is just a constant, while the second term provides the non-interacting (linear) SW spectrum. In fact, the eigenvalues of $\chi(\mathbf{q})$ are the discrete SW energies $E_{\mathbf{q},\nu}$ where $\nu = 1, 2, \ldots, N$ is a branch label (each eigenvalue will occur *twice* in $\chi(\mathbf{q})$). Results for $E_{\mathbf{q},\nu}$ have already been obtained using the equivalent determinantal condition in Eq. (10). We now diagonalize $H^{(2)}$ by making a linear transformation to a new set of boson operators $\alpha_{\mathbf{q}}^{\dagger}$ and $\alpha_{\mathbf{q}}$, which satisfy the usual commutation relations and are defined by

$$a_{\mathbf{q},n} = \sum_{l} S_{nl}\left(\mathbf{q}\right) \alpha_{\mathbf{q},l} + T_{nl}^{*}\left(\mathbf{q}\right) \alpha_{-\mathbf{q},l}^{\dagger}, \tag{20}$$

$$a_{\mathbf{q},n}^{\dagger} = \sum_{l} S_{nl}^{*}\left(\mathbf{q}\right) \alpha_{\mathbf{q},l}^{\dagger} + T_{nl}\left(\mathbf{q}\right) \alpha_{-\mathbf{q},l}. \tag{21}$$

The S_{nl} and T_{nl} coefficients can be found by a straightforward generalization of a procedure due to White et al,[22] and the result is as follows. Suppose we rewrite the above transformation in matrix form as $\tilde{\mathcal{A}}_{\mathbf{q}}^{\dagger} = S_{\mathbf{q}}^{*}\Lambda_{\mathbf{q}}^{\dagger}$ and $\mathcal{A}_{\mathbf{q}} = S_{\mathbf{q}}\Lambda_{\mathbf{q}}$, where $\Lambda_{\mathbf{q}}^{\dagger}$ and $\Lambda_{\mathbf{q}}$ are defined similarly to $\mathcal{A}_{\mathbf{q}}^{\dagger}$ and $\mathcal{A}_{\mathbf{q}}$ but in terms of the new operators. The jth column (denoted by $S_{j,\mathbf{q}}$) of the $2N \times 2N$ transformation matrix $S_{\mathbf{q}}$ is then found by solving for the eigenvector in

$$\begin{pmatrix} \tilde{\mathbf{A}}^{(2)}\left(\mathbf{q}\right) & 2\tilde{\mathbf{C}}^{(2)}\left(\mathbf{q}\right) \\ -2\tilde{\mathbf{B}}^{(2)}\left(-\mathbf{q}\right) & -\mathbf{A}^{(2)}\left(-\mathbf{q}\right) \end{pmatrix} \mathbf{S}_{j,\mathbf{q}} = \pm\epsilon_{j}\left(\mathbf{q}\right) \mathbf{S}_{j,\mathbf{q}}, \tag{22}$$

where the $+$ sign is taken for $j \in 1, \ldots, N$ and the $-$ sign for $j \in N+1, \ldots, 2N$. The $H^{(2)}$ part of the Hamiltonian then assumes the simple form (apart from a constant term):

$$H^{(2)} = \sum_{\mathbf{q}\nu} E_{\mathbf{q},\nu}(1 + 2\alpha_{\mathbf{q}\nu}^{\dagger}\alpha_{\mathbf{q}\nu}). \tag{23}$$

To establish the diagram technique we now introduce a $N \times N$ matrix $\mathbf{G}(\mathbf{q}, i\omega_m)$ with matrix elements defined as the causal Green functions involving the transformed boson operators:

$$G_{\nu\nu'}(\mathbf{q}, i\omega_m) = \left\langle\left\langle \alpha_{\mathbf{q}\nu}; \alpha^{\dagger}_{\mathbf{q}\nu'} \right\rangle\right\rangle_{i\omega_m}. \tag{24}$$

in a conventional notation.[13] Here $i\omega_m \equiv 2\pi m i/\beta$ is an imaginary boson frequency, where $\beta = 1/k_B T$ and m takes all integer values from $-\infty$ to $+\infty$. When these Green functions are evaluated using just $H^{(2)}$ in Eq. (23) for the Hamiltonian the resulting non-interacting Green functions are diagonal in the labels ν and ν' and are given by

$$G^0_{\nu\nu'}(\mathbf{q}, i\omega_m) = G^0_{\nu}(\mathbf{q}, i\omega_m)\delta_{\nu,\nu'} = \left(-\frac{1}{\beta}\right)\frac{1}{i\omega_m - E_{\mathbf{q},\nu}}\delta_{\nu,\nu'}. \tag{25}$$

On making an analytic continuation $i\omega_m \rightarrow \omega + i0^+$ to real frequency ω, it is seen that there is a simple pole at the values $E_{\mathbf{q},\nu}$. These correspond to the non-interacting excitations, comprising the discrete bulk and surface SW modes, which we have already been in the linear case. In the higher orders of perturbation, i.e. when $H^{(3)}$ and $H^{(4)}$ are included, the "interacting" (or renormalized) Green functions will have modified poles, corresponding to a renormalization in energy by an amount $\Delta E_{\mathbf{q},\nu}$ and a damping $\Gamma_{\mathbf{q},\nu}$. Also, in general, the interacting Green functions will have off-diagonal terms in the ν and ν' labels. As in standard diagrammatic formulations for interacting boson systems, the interacting and non-interacting Green functions are related to one another by means of the Dyson development operator.[23] This quantity can be expanded as an infinite series in powers of the higher-order Hamiltonian parts. The terms in the expansion can conveniently be evaluated using a diagrammatic representation with proper self-energy terms $\Sigma_{\nu\nu'}(\mathbf{q}, i\omega_m)$ introduced to account for the interactions. The choice of the self-energy terms within the perturbation expansion depends on the explicit form of $H^{(3)}$ and $H^{(4)}$ and will be discussed in the following sections.

First, the non-interacting Green function $G^0_{\nu\nu'}(\mathbf{q}, i\omega_m)$ will be drawn as a solid directed line as shown in Fig. 3(a). There are then four possible types of proper self-energy terms,

as defined in Fig. 3(b), depending on whether the G^0 lines are entering or leaving. All of these may be nonzero when there are magnetic dipole-dipole contributions to the Hamiltonian. The renormalized Green functions are given by a generalized Dyson series, which is represented diagrammatically in Fig. 4. This takes the algebraic form

$$\begin{aligned} G_{\nu\nu'}(\mathbf{q}, i\omega_m) = {} & G^0_\nu(\mathbf{q}, i\omega_m)\delta_{\nu\nu'} + G^0_\nu(\mathbf{q}, i\omega_m)\Sigma^{+-}_{\nu\nu'}(\mathbf{q}, i\omega_m)G^0_{\nu'}(\mathbf{q}, i\omega_m) \\ & + \sum_{\nu''} G^0_\nu(\mathbf{q}, i\omega_m)\Sigma^{+-}_{\nu\nu''}(\mathbf{q}, i\omega_m)G^0_{\nu''}(\mathbf{q}, i\omega_m)\Sigma^{+-}_{\nu''\nu'}(\mathbf{q}, i\omega_m)G^0_{\nu'}(\mathbf{q}, i\omega_m) \\ & + \sum_{\nu''} G^0_\nu(\mathbf{q}, i\omega_m)\Sigma^{++}_{\nu\nu''}(\mathbf{q}, i\omega_m)G^0_{\nu''}(\mathbf{q}, i\omega_m)\Sigma^{--}_{\nu''\nu'}(\mathbf{q}, i\omega_m)G^0_{\nu'}(\mathbf{q}, i\omega_m) + ... \end{aligned} \quad (26)$$

We note that the only term linear in the self-energy parts is the one involving Σ^{+-}. The terms with Σ^{++} and Σ^{--} occur in diagrams quadratic (and higher) in the self-energy parts, and Σ^{-+} occurs only in diagrams that are cubic and higher. If we ignore, for the moment, the effects of Σ^{++}, Σ^{--}, and Σ^{-+}, the infinite Dyson equation series for $G_{\nu\nu'}(\mathbf{q}, i\omega_m)$ is summable, and the formal solution can be written in a matrix form as

$$\mathbf{G}(\mathbf{q}, i\omega_m) = \mathbf{G}^0(\mathbf{q}, i\omega_m) + \mathbf{G}^0(\mathbf{q}, i\omega_m)\mathbf{\Sigma}^{+-}(\mathbf{q}, i\omega_m)\mathbf{G}(\mathbf{q}, i\omega_m). \quad (27)$$

The solution of this matrix equation is

$$\mathbf{G}(\mathbf{q}, i\omega_m) = \left\{ \left[\mathbf{G}^0(\mathbf{q}, i\omega_m)\right]^{-1} - \mathbf{\Sigma}^{+-}(\mathbf{q}, i\omega_m) \right\}^{-1}. \quad (28)$$

By solving for the complex poles of this interacting Green function we may deduce the renormalized SW energies $\Delta E_{\mathbf{q},\nu}$ and their damping $\Gamma_{\mathbf{q},\nu}$. The condition is

$$\det \left\{ \left[\mathbf{G}^0(\mathbf{q}, i\omega_m)\right]^{-1} - \mathbf{\Sigma}^{+-}(\mathbf{q}, i\omega_m) \right\} = 0. \quad (29)$$

After substituting for the matrix elements of $[\mathbf{G}^0(\mathbf{q}, i\omega_m)]^{-1}$ using Eq. (25) this becomes

$$\begin{vmatrix} E_{\mathbf{q},1} - i\omega_m - \frac{1}{\beta}\Sigma^{+-}_{11}(\mathbf{q}, i\omega_m) & \frac{1}{\beta}\Sigma^{+-}_{12}(\mathbf{q}, i\omega_m) & \cdots\cdots \\ \frac{1}{\beta}\Sigma^{+-}_{21}(\mathbf{q}, i\omega_m) & E_{\mathbf{q},2} - i\omega_m - \frac{1}{\beta}\Sigma^{+-}_{22}(\mathbf{q}, i\omega_m) & \cdots\cdots \\ \vdots & \vdots & \ddots \end{vmatrix} = 0. \quad (30)$$

At low temperatures $T \ll T_C$, where the perturbative expansion is expected to be good, an approximation to Eq. (30) (and hence to ΔE and Γ for each SW branch) may be obtained

by expanding the determinant to lowest order in the off-diagonal elements. The results may eventually be expressed as

$$\Delta E_{\mathbf{q},\nu} + i\Gamma_{\mathbf{q},\nu} = -\frac{1}{\beta}\Sigma^{+-}_{\nu\nu}(\mathbf{q}, E_{\mathbf{q},\nu} + i0^+) + O[\Sigma^{+-}_{\nu\nu'}(\mathbf{q}, E_{\mathbf{q},\nu} + i0^+)]^2, \tag{31}$$

where $\nu' \neq \nu$. In deriving Eq. (31) we have assumed that $|\Delta E + i\Gamma| \ll E$, and so the matrix elements are evaluated there at the unrenormalized SW energy.

When the other types of self-energy terms (i.e., Σ^{++}, Σ^{--}, and Σ^{-+}) are taken into account, it is found that they modify Eq. (31) only by adding terms of second order (and higher) on the right-hand side. Therefore, to leading order (neglecting the quadratic self-energy terms) we have

$$\Delta E_{\mathbf{q},\nu} \simeq -\frac{1}{\beta}\mathrm{Re}\ \Sigma^{+-}_{\nu\nu}(\mathbf{q}, E_{\mathbf{q},\nu} + i0^+), \tag{32}$$

$$\Gamma_{\mathbf{q},\nu} \simeq -\frac{1}{\beta}\mathrm{Im}\ \Sigma^{+-}_{\nu\nu}(\mathbf{q}, E_{\mathbf{q},\nu} + i0^+), \tag{33}$$

for the energy shift and damping, respectively, of SW branch ν at in-plane wave vector $\mathbf{q}$. In the following sections the above expressions are used to study the effects of the three- and four-magnon interaction processes.

VI. THREE- AND FOUR-MAGNON PROCESSES

A. Three-Magnon Processes

The term $H^{(3)}$ in the expansion of the Hamiltonian is given in Eq. (11). It arises entirely from the dipole-dipole interactions and is of third order in the boson operators. It describes splitting processes, in which one magnon is absorbed and two are emitted, and confluence processes, in which two magnons are absorbed and one magnon is emitted. These can lead to transfers of energy between the different SW branches (surface and quantized bulk modes).

The first step is to rewrite $H^{(3)}$ in terms of the new boson operators $\alpha^\dagger_{\mathbf{q}}$ and $\alpha_{\mathbf{q}}$ using Eqs. (20) and (21), so that the diagrammatic formalism may be employed. The result is

$$H^{(3)} = \frac{1}{2}\sum_{l_1 l_2 l_3 \mathbf{k}\mathbf{q}} \Big[V_1\, \alpha^{\dagger}_{\mathbf{k},l_1}\alpha^{\dagger}_{\mathbf{q}-\mathbf{k},l_2}\alpha_{\mathbf{q},l_3} + V_2\, \alpha^{\dagger}_{\mathbf{q},l_1}\alpha_{\mathbf{q}-\mathbf{k},l_2}\alpha_{\mathbf{k},l_3} + V_3\, \alpha^{\dagger}_{\mathbf{k},l_1}\alpha^{\dagger}_{\mathbf{q}-\mathbf{k},l_2}\alpha^{\dagger}_{-\mathbf{q},l_3} + V_4\, \alpha_{-\mathbf{q},l_1}\alpha_{\mathbf{q}-\mathbf{k},l_2}\alpha_{\mathbf{k},l_3} \Big], \tag{34}$$

where the amplitude factors V_i (with $i = 1, 2, 3, 4$) are listed in Appendix B. The leading-order diagrammatic contributions to the proper self-energy term Σ^{+-}_{ll}, as required for the renormalization of any SW branch l, are shown in Fig. 5. Each of the dotted lines represents a V_i (as an "interaction vertex") according to the direction of arrowing on the three Green-function lines entering or leaving it (e.g., a V_4 vertex has three lines leaving). All of the diagrams in Fig. 5 are of second order in the vertices. Using the formal rules of diagrammatic evaluation for interacting boson systems,[23] we obtain the self-energy expression as

$$\Sigma_{ll}(\mathbf{q}, i\omega_m) = -\beta \sum_{\mathbf{q}'l'l''} \left\{ (W_a + W_b)\frac{n^0(E_{\mathbf{q}',l'})}{E_{\mathbf{q},l''}} + W_c \frac{n^0(E_{\mathbf{q}',l'}) + n^0(E_{-\mathbf{q}-\mathbf{q}',l''}) + 1}{E_{-\mathbf{q}-\mathbf{q}',l''} + E_{\mathbf{q}',l'} + i\omega_m} + W_d \frac{n^0(E_{\mathbf{q}',l'}) + n^0(E_{\mathbf{q}-\mathbf{q}',l''}) + 1}{E_{\mathbf{q}-\mathbf{q}',l''} + E_{\mathbf{q}',l'} - i\omega_m} + W_e \frac{n^0(E_{\mathbf{q}',l'}) - n^0(E_{\mathbf{q}+\mathbf{q}',l''})}{E_{\mathbf{q}+\mathbf{q}',l''} - E_{\mathbf{q}',l'} - i\omega_m} \right\}. \tag{35}$$

The weighting factors $W_{a,b,\ldots,e}$ are given in Appendix B and $n^0(E) \equiv [\exp(\beta E) - 1]^{-1}$ denotes the Bose-Einstein thermal factor at energy E. Next, using Eqs. (32) and (33), together with the well-known relation

$$\frac{1}{(x \pm iE)} = \mathrm{P}\left(\frac{1}{x}\right) \mp i\pi\delta(x), \tag{36}$$

where P indicates that the principal value is taken in a summation over x, we obtain

$$\Delta E_{\mathbf{q},l} = \mathrm{P}\sum_{\mathbf{q}'l'l''} \left\{ (W_a + W_b)\frac{n^0(E_{\mathbf{q}',l'})}{E_{\mathbf{q},l''}} + W_c \frac{n^0(E_{\mathbf{q}'l'}) + n^0(E_{-\mathbf{q}-\mathbf{q}',l''}) + 1}{E_{-\mathbf{q}-\mathbf{q}',l''} + E_{\mathbf{q}',l'} + E_{\mathbf{q},l}} + W_d \frac{n^0(E_{\mathbf{q}'l'}) + n^0(E_{\mathbf{q}-\mathbf{q}',l''}) + 1}{E_{\mathbf{q}-\mathbf{q}',l''} + E_{\mathbf{q}',l'} - E_{\mathbf{q},l}} + W_e \frac{n^0(E_{\mathbf{q}',l'}) - n^0(E_{\mathbf{q}+\mathbf{q}',l''})}{E_{\mathbf{q}+\mathbf{q}',l''} - E_{\mathbf{q}',l'} - E_{\mathbf{q},l}} \right\}. \tag{37}$$

for the energy shift, and

$$\Gamma_{\mathbf{q},l} = -\pi \sum_{\mathbf{q}'l'l''} \Big\{ W_d \left[n^0(E_{\mathbf{q}',l'}) + n^0(E_{\mathbf{q}-\mathbf{q}',l''}) + 1 \right] \delta(E_{\mathbf{q}-\mathbf{q}',l''} + E_{\mathbf{q}',l'} - E_{\mathbf{q},l}) + W_d \left[n^0(E_{\mathbf{q}',l'}) - n^0(E_{\mathbf{q}+\mathbf{q}',l''}) \right] \delta(E_{\mathbf{q}+\mathbf{q}',l''} - E_{\mathbf{q}',l'} - E_{\mathbf{q},l}) \Big\}, \tag{38}$$

for the damping. The two delta functions in Eq. (38), which conserve energy and in-plane wave vector, correspond to the three-magnon splitting and confluence processes respectively. The applications of the above results for ΔE and Γ are discussed in Sec. VII.

B. Four-Magnon Processes

Following the previous section we first rewrite the interaction Hamiltonian, in this case the four-magnon contribution $H^{(4)}$ given by Eq. (13), in terms of the new boson operators. After a straightforward but lengthy calculation we obtain the following expression:

$$\begin{aligned} H^{(4)} = \frac{1}{2} \sum_{l_1 l_2 l_3 l_4 \mathbf{k}\mathbf{k}'\mathbf{q}} \Big\{ & \Lambda_1 \alpha^\dagger_{\mathbf{k}' l_1} \alpha^\dagger_{\mathbf{q}-\mathbf{k}', l_2} \alpha_{\mathbf{q}-\mathbf{k}, l_3} \alpha_{\mathbf{k}, l_4} + \Lambda_2 \alpha^\dagger_{\mathbf{q} l_1} \alpha_{\mathbf{q}-\mathbf{k}-\mathbf{k}', l_2} \alpha_{\mathbf{k}', l_3} \alpha_{\mathbf{k}, l_4} \\ & + \Lambda_3 \alpha^\dagger_{\mathbf{k}'_1} \alpha^\dagger_{\mathbf{k}', l_2} \alpha^\dagger_{\mathbf{q}-\mathbf{k}-\mathbf{k}', l_3} \alpha_{\mathbf{q}, l_4} + \Lambda_4 \alpha^\dagger_{\mathbf{k}' l_1} \alpha^\dagger_{\mathbf{q}-\mathbf{k}', l_2} \alpha^\dagger_{\mathbf{k}-\mathbf{q}, l_3} \alpha^\dagger_{-\mathbf{k}, l_4} \\ & + \Lambda_5 \alpha_{-\mathbf{k}' l_1} \alpha_{\mathbf{k}'-\mathbf{q}, l_2} \alpha_{\mathbf{q}-\mathbf{k}, l_3} \alpha_{\mathbf{k}, l_4} \Big\} , \end{aligned} \tag{39}$$

where the amplitude factors Λ_i $(i = 1, 2, 3, 4)$ associated with each operator term are given in Appendix C. These terms define the interaction vertices of the diagrammatic formalism. By contrast to the three-magnon case, the four-magnon interactions involve dipolar and exchange terms and contribute even in the Heisenberg limit (see, e.g., Kontos and Cottam[15,16] for the case of a semi-infinite Heisenberg ferromagnet).

According to Eqs. (32) and (33), the formal results for the SW energy shift and damping related to $H^{(4)}$ arise from the real and imaginary parts, respectively, of an appropriately-chosen self energy term in the Λ_i vertices. The leading-order contribution (denoted by $\Sigma^{(1)}$) to the proper self-energy $\Sigma^{+-}(\mathbf{q}, i\omega_m)$ is of first order in Λ_i and corresponds to the diagram in Fig. 6a, together with topologically similar diagrams. Again the dotted line represents an interaction vertex corresponding to the number of lines entering or leaving. On evaluating the diagrams we obtain the contribution to the energy shift of SW branch l as

$$\Delta E_{\mathbf{q},l} = \sum_{\mathbf{q}' l'} \Theta_a n^0(E_{\mathbf{q}', l'}) \tag{40}$$

where the weighting term Θ_a arises from a combination of Λ_1 vertices and is defined in Appendix C. It is the analog, for the thin film with exchange and dipolar coupling, of the Dyson SW interaction term for the case of bulk SW in an infinite Heisenberg ferromagnet (see, e.g., Ref. 12).

It turns out that the self-energy part $\Sigma^{(1)}$ is real, and so it gives a vanishing contribution

to the damping. Therefore, to calculate the damping, it is necessary to consider the self-energy contributions $\Sigma^{(2)}$ that are of *second* order in the Λ_i vertices. This corresponds to diagrams with a more complicated loop structure (and hence with more internal variables). In Fig. 6b we show just those diagrams for $\Sigma^{(2)}$ that give rise to a damping term (i.e., those that have an imaginary part after the analytic continuation $i\omega_m \to E_{\mathbf{q},l} + i0^+$ is made. The final result for the damping of SW branch l is

$$\begin{aligned}\Gamma_{\mathbf{q},l} = -\pi \sum_{\mathbf{q}'\mathbf{q}''l'l''l'''} \Big\{ & \Theta_b \Big\{ n^0(E_{\mathbf{q}'-\mathbf{q},l'}) \Big[n^0(E_{\mathbf{q}'',l''}) + 1 \Big] - n^0(E_{\mathbf{q}'-\mathbf{q}'',l'''}) \\ & \times [\, n^0(E_{\mathbf{q}'',l''}) - n^0(E_{\mathbf{q}'-\mathbf{q},l'}) \,] \Big\} \, \delta \left(E_{\mathbf{q}'',l''} + E_{\mathbf{q}'-\mathbf{q}'',l'''} - E_{\mathbf{q}'-\mathbf{q},l'} - E_{\mathbf{q},l} \right) \\ & + \Theta_c \Big\{ n^0(E_{\mathbf{q}'',l''}) n^0(E_{\mathbf{q}'-\mathbf{q}'',l'''}) + \Big[n^0(E_{\mathbf{q}'',l''}) + 1 \Big] \\ & \times \Big[n^0(E_{\mathbf{q}'',l''}) + n^0(E_{\mathbf{q}'-\mathbf{q}'',l'''}) + 1 \Big] \Big\} \, \delta \left(E_{\mathbf{Q}'',l''} + E_{\mathbf{q}-\mathbf{q}',l'} + E_{\mathbf{q}'-\mathbf{q}'',l'''} - E_{\mathbf{q},l} \right) \\ & + \Theta_d \Big\{ n^0(E_{\mathbf{q}'-\mathbf{q},l'}) \times \Big[n^0(E_{\mathbf{q}'',l''}) + 1 \Big] - n^0(E_{\mathbf{q}'-\mathbf{q},l'}) \\ & \times [\, n^0(E_{\mathbf{q}'',l''}) - n^0(E_{\mathbf{q}'-\mathbf{q},l'}) \,] \Big\} \, \delta \left(E_{\mathbf{q}'+\mathbf{q}'',l'''} - E_{\mathbf{q}'',l''} - E_{\mathbf{q}'-\mathbf{q},l'} - E_{\mathbf{q},l} \right) \Big\} . \end{aligned} \tag{41}$$

The second-order weighting factors $\Theta_{b,c,d}$, which multiply the three different delta functions conserving energy and in-plane wave vector, are given in Appendix C.

VII. NUMERICAL RESULTS AND DISCUSSION

Numerical calculations for particular materials are now presented based on the formal expressions for $\Delta E_{\mathbf{q},l}$ and $\Gamma_{\mathbf{q},l}$ in the previous section. This provides us with predictions of the overall dependence on $\mathbf{q}$ and T for the different SW branches and allows us to compare the relative importance of the three- and four-magnon processes in various situations.

We start by considering ultrathin films of EuO, where the dipolar interactions have a significant effect on the long-wavelength linear SW properties and the exchange effects dominate at shorter wavelengths (see Sec. III). We assume the same values for $4\pi M$ and H_{Ex} as before, but for simplicity we ignore the next-nearest exchange J_2. In Fig. 7a we show the damping of the lowest SW branch (labeled 1) for $N = 8$ and for temperature $T \ll T_C$ as a function of the in-plane wave-vector component q_x. The mode under consideration is

the analog of the DE surface mode at small q_x which is then modified by the exchange at larger q_x. In this case it is found that the dominant damping mechanism comes from the three-magnon term $H^{(3)}$ in second order, i.e., from Eq. (38). The delta functions in Eq. (38) give $E_{\mathbf{q},l} = E_{\mathbf{q}\mp\mathbf{q}',l''} \pm E_{\mathbf{q}',l'}$, in accordance with conservation of energy and in-plane wave vector. For a SW with in-plane wave vector $\mathbf{q}$ and branch l, these correspond physically to the splitting (upper signs) and confluence (lower signs) processes. Here the labels l' and l'' may be the same as, or different from, l. Along with the total three-magnon damping contribution (solid curve) we show in Fig. 7a the contributions from some of individual (l', l'') processes. It is seen that several of the inter-branch processes (i.e., where at least one of l' and l'' differs from l) play an important role. In Fig. 7b we make some comparisons between the total damping for the SW branch 1 with $N = 8$ (solid curve) and $N = 16$ (dotted line). In this particular case the damping has a similar behavior for both values of N, although the individual inter-branch contributions (not shown) are different. In the same plot we show the total damping for branch 2 in the case of $N = 8$ (dashed curve). This is slightly larger than the damping for branch 1, mainly because there are SW branches above and below it, giving more possibilities to satisfy the required conservation conditions.

It is interesting to compare the damping results predicted for EuO with those for other materials. We consider Fe where the ratio of dipolar to exchange strength is smaller than in EuO, as well as $GdCl_3$ where the ratio is larger. For the case of a $GdCl_3$ film with $N = 8$ layers, the total damping at $T \ll T_C$ is shown in Fig. 8, where we use the same $4\pi M$ and H_{Ex} as in Sec. III. This presents a rather different behavior, particularly for small q_x, when compared to a EuO film (see Fig. 7a) and also to a Fe film (see Fig. 9). The parameters used for the latter case are $4\pi M = 2.14$ T and $H_{Ex} = 2140$ T. The qualitative differences for the dominant three-magnon damping in the case of $GdCl_3$ is mainly because the influence of the dipolar terms (including the role of the DE surface mode) extends over a greater range of wave vectors than is the case for EuO or Fe. This makes it easier to satisfy the energy and wave-vector conservation conditions for the damping at smaller wave vectors.

As mentioned earlier, the three-magnon damping has contributions due to splitting and

confluence processes. The temperature dependence of these processes arise from the combinations of Bose factors associated with each delta-function term. We note, in particular, that the second term (the confluence term) on the right-hand side of Eq. (38) vanishes as $T \to 0$. This is as expected since there needs to be a thermally-excited SW to participate in the confluence. By contrast, the first term in Eq. (38) does not vanish in the zero-temperature limit, since it is always possible (provided the conservation conditions are satisfied) for a SW to split into two modes. The numerical calculations presented above were all for the low-temperature limit where the three-magnon splitting is dominant. In Fig. 10 we show calculations for the temperature dependence of the three-magnon damping, taking the case of a EuO film (with the same parameters as in Fig. 7a) and a fixed value of the wave-vector component ($q_x/\pi = 0.5$). It can be seen that, at low enough temperatures, the splitting process (solid curve) dominates and increases slowly with temperature, whereas the confluence process (dashed curve) increases very rapidly with temperature.

The four-magnon damping, which is given by Eq. (41), contains three different processes proportional to the weighting factors Θ_b, Θ_c and Θ_d, together with their Bose factors. The delta functions provide for conservation of energy and in-plane wave vectors. The only non-vanishing contribution as $T \to 0$ is the term proportional to Θ_c, which describes a splitting of an incoming SW into *three* modes. It is proportional to the dipole-dipole sums (i.e., it vanishes in the exchange limit) and is generally less important than the splitting process in Eq. (38) discussed above. The other two terms in Eq. (41) contribute to the four-magnon damping when $T \neq 0$. The first term (proportional to Θ_b) is the analog of the scattering term in the damping for Heisenberg systems.[12,15,16] The incoming SW scatters off a thermally-excited SW into two other SW modes. The term proportional to Θ_d corresponds to the incoming SW scattering off a pair of SW modes into another SW mode. It arises specifically as a consequence of the dipolar terms in the Hamiltonian.

We now turn to a discussion of results for the SW energy shifts, which are given by Eqs. (37) and (40) for the three- and four-magnon cases respectively. In a low-temperature limit $T \ll T_C$ the dominant contributions come from the three-magnon processes, specifically

from the terms proportional to W_c and W_d in Eq. (37). Numerical results for $\Delta E_{\mathbf{q},l}$ versus q_x for EuO films in the same three cases as Fig. 7b are shown in Fig. 11. The main difference (compared to the damping) is that the inter-branch terms are much more important. This arises basically as a consequence of $\Delta E_{\mathbf{q},l}$ and $\Gamma_{\mathbf{q},l}$ coming from the real and imaginary parts, respectively, of self-energy terms in the diagram formalism, and these may have quite different dependencies. For example, the imaginary parts have delta functions, which lead to peaks and structural features in the damping, whereas the summations in the real parts tend to give a smoother behavior for the SW energy shifts. Hence ΔE has a weaker dependence on q_x in Fig. 11 than was the case for the damping. The larger ΔE value and its q_x-dependence for the thicker film (where the linear SW modes are closer together) is due to the inter-branch terms in the summations.

At low but finite temperatures with $T \ll T_C$ the four-magnon contribution to $\Delta E_{\mathbf{q},l}$ begins to play a role, particularly for the lower-energy SW branches, because the Bose factor in Eq. (40) becomes nonzero. Some numerical calculations are shown in Figs. 12 and 13 for EuO films with $N = 8$. In Fig. 12 the four-magnon contribution to the energy shift for the lowest SW branch ($l = 1$) is plotted as a function of wave-vector component q_x at a fixed temperature ($T = 0.04$ K). It is seen that the qualitative behavior is quite different from that for the three-magnon contribution (see Fig.11). We note also that the q_x-dependence in Fig. 12 is different from that of the four-magnon energy shift for a Heisenberg ferromagnet,[12,15,16] which is proportional to q_x^2 at small wave vectors. This difference, compared to Heisenberg systems, is partly due to the the dipolar terms in the factor Θ_a in Eq. (40) and partly due to the dipolar contribution to the SW energy gap. In Fig. 13 we compare the temperature dependence of the three-magnon SW energy shift (solid curve) with that due to four-magnon processes (dashed curve). The latter quantity increases rapidly with temperature and eventually dominates. This is again for a EuO film, but for a fixed wave vector corresponding to $q_x = 0.5\pi$.

VIII. CONCLUSIONS

We have developed a microscopic (Hamiltonian-based) theory for the dipole-exchange SW modes and the interactions between them in ultrathin ferromagnetic films. We first used the theory to study the linear dispersion relation of the discrete SW in EuO and $GdCl_3$, including the effects of next-nearest neighbor exchange. The results obtained with the microscopic theory are in good agreement with those of the usual macroscopic theories in limiting cases where there are a large number of layers and the wave vectors are very small. Outside of these regimes it becomes necessary to use a microscopic approach, as in this work.

Secondly, the theory enabled us to develop the leading-order three- and four-magnon interaction terms in the Hamiltonian for the film. These three- and four-magnon processes can involve modes from the different discrete SW branches (surface or bulk) in all combinations. Formal expressions were found for the energy shift and damping of each branch. Applications were made to EuO, Fe, and $GdCl_3$. In the case where the three-magnon processes dominate, it has been shown that there are significantly different types of behavior predicted for $GdCl_3$ compared to EuO or Fe. This happens because the influence of the dipolar terms extends over a greater range of wave vectors in the $GdCl_3$. As a consequence, the energy and wave-vector conservation conditions for the damping are more readily satisfied at smaller wave vectors. Our method enabled us to carry out calculations also at higher temperatures, where the four-magnon processes play a more significant role. The above-mentioned influence of the dipolar interactions also makes an important contribution to these processes. The major effect, compared to the four-magnon energy shift in a Heisenberg ferromagnet without dipolar interactions, can be observed in the q_x dependence of the four-magnon energy shift.

In order to probe the effects discussed here, inelastic light scattering would be an appropriate experimental technique.[19] An interesting extension of our work would be to apply the nonlinear theory in an examination of SW instabilities in ultrathin films under conditions

of parallel or perpendicular "pumping" by a microwave field.

ACKNOWLEDGMENTS

The authors gratefully acknowledge partial support from NSERC (Canada) and the Brazilian agencies CNPq, CAPES, FINEP, and FUNCAP.

APPENDIX A: DIPOLE SUMS

Here we list the expressions and properties of the dipole sums required for this work. They are calculated as in Ref. 8.

The sums of dipole interactions between spins located in *different* atomic layers (i.e., with $y \equiv \|(n-n')\| \neq 0$) have the following expressions:

$$D^{xx}_{n,n'}(q_x,q_z) = 4\pi \sum_{l,m=-\infty}^{\infty} \frac{(\pi l + q_x/2)^2}{\gamma_{lm}} \exp\left(-2\left|y\right|\gamma_{lm}\right), \tag{A1}$$

$$D^{yy}_{n,n'}(q_x,q_z) = -4\pi \sum_{l,m=-\infty}^{\infty} \gamma_{lm} \ \exp\left(-2\left|y\right|\gamma_{lm}\right), \tag{A2}$$

$$D^{zz}_{n,n'}(q_x,q_z) = 4\pi \sum_{l,m=-\infty}^{\infty} \frac{(\pi m + q_z/2)^2}{\gamma_{lm}} \exp\left(-2\left|y\right|\gamma_{lm}\right), \tag{A3}$$

$$D^{xy}_{n,n'}(q_x,q_z) = -i4\pi sgn(y) \sum_{l,m=-\infty}^{\infty} (\pi l + q_x/2) \exp\left(-2\left|y\right|\gamma_{lm}\right), \tag{A4}$$

$$D^{zy}_{n,n'}(q_x,q_z) = -i4\pi sgn(y) \sum_{l,m=-\infty}^{\infty} (\pi m + q_z/2) \exp\left(-2\left|y\right|\gamma_{lm}\right), \tag{A5}$$

$$D^{xz}_{n,n'}(q_x,q_z) = 4\pi \sum_{l,m=-\infty}^{\infty} \frac{(\pi l + q_x/2)(\pi m + q_z/2)}{\gamma_{lm}} \exp\left(-2\left|y\right|\gamma_{lm}\right). \tag{A6}$$

In the expressions above we denote $\gamma_{lm} = [(\pi l + q_x/2)^2 + (\pi m + q_z/2)^2]$, and $K_i(x)$ is a modified Bessel function of integer order i for any variable x.

For the dipolar sums involving spins in the *same* layer ($y = 0$) we have the following expressions for the diagonal terms (involving the same superscript):

$$D_{n,n}^{xx}(q_x, q_z) = -2S_x(q_x, q_y) + S_z(q_x, q_y), \tag{A7}$$

$$D_{n,n}^{yy}(q_x, q_z) = S_x(q_x, q_y) + S_z(q_x, q_y), \tag{A8}$$

$$D_{n,n}^{zz}(q_x, q_z) = -2S_z(q_x, q_y) + S_x(q_x, q_y), \tag{A9}$$

where

$$S_x(q_x, q_y) = \frac{16}{3}\sum_{x=1}^{\infty}\sum_{m=-\infty}^{\infty}(\pi m + q_z/2)^2 \cos(q_x x)\left[K_2(2x|\pi m + q_z/2|)\right], \tag{A10}$$

$$S_z(q_x, q_y) = \frac{16}{3}\sum_{z=1}^{\infty}\sum_{m=-\infty}^{\infty}(\pi m + q_x/2)^2 \cos(q_z z)\left[K_2(2z|\pi m + q_x/2|)\right]. \tag{A11}$$

Also for the off-diagonal terms:

$$D_{n,n}^{xz}(q_x, q_z) = 16\sum_{x=1}^{\infty}\sum_{m=-\infty}^{\infty}(\pi m + q_z/2)|\pi m + q_z/2|\sin(q_x x)\left[K_1(2x|\pi m + q_z/2|)\right], \tag{A12}$$

while $D_{n,n}^{xy}(q_x, q_z) = D_{n,n}^{yz}(q_x, q_z) = 0$ by symmetry. Finally, when $q_x = q_z = 0$, we have

$$D_{n,n}^{zz}(0, 0) = -\frac{4\pi^2}{9}\left[1 + 24\sum_{m=1}^{\infty} m^2 K_2(2x\pi m)\right]. \tag{A13}$$

APPENDIX B: THREE-MAGNON AMPLITUDE FACTORS

The expressions for the amplitude factor V_i ($i = 1, 2, 3, 4$) in Eq. (34), and hence for the vertices in the diagrammatic representation, are given by

$$\begin{aligned}
V_1(\mathbf{k}, \mathbf{q}|l_1, l_2, l_3) = \sum_{nn'}\Big\{ & A_{nn'}^{(3)}(\mathbf{k}) S_{n'l_1}^*(\mathbf{k}) S_{nl_2}^*(\mathbf{q}-\mathbf{k}) S_{nl_3}(\mathbf{q}) \\
& + A_{nn'}^{(3)}(\mathbf{k}) S_{n'l_1}^*(\mathbf{k}) T_{nl_2}^*(\mathbf{k}-\mathbf{q}) T_{nl_3}(\mathbf{q}) \\
& + A_{nn'}^{(3)}(-\mathbf{k}) T_{n'l_1}^*(-\mathbf{k}) S_{nl_2}^*(\mathbf{q}-\mathbf{k}) S_{nl_3}(\mathbf{q}) \\
& + A_{nn'}^{(3)}(-\mathbf{k}) T_{n'l_1}^*(-\mathbf{k}) T_{nl_2}^*(\mathbf{k}-\mathbf{q}) T_{nl_3}(-\mathbf{q}) \\
& + A_{nn'}^{(3)}(-\mathbf{q}) T_{nl_1}^*(-\mathbf{k}) S_{nl_2}^*(\mathbf{q}-\mathbf{k}) T_{n'l_3}(-\mathbf{q}) \\
& + A_{nn'}^{(3)}(\mathbf{q}) S_{nl_1}^*(\mathbf{k}) T_{nl_2}^*(\mathbf{k}-\mathbf{q}) S_{n'l_3}(\mathbf{q})\Big\},
\end{aligned} \tag{B1}$$

$$V_2(\mathbf{k},\mathbf{q}|l_1,l_2,l_3) = \sum_{nn'} \Big\{ A^{(3)}_{nn'}(\mathbf{k}) S^*_{nl_1}(\mathbf{q}) S_{nl_2}(\mathbf{q}-\mathbf{k}) S_{n'l_3}(\mathbf{k}) + A^{(3)}_{nn'}(\mathbf{k}) T^*_{nl_1}(-\mathbf{q}) T_{nl_2}(\mathbf{k}-\mathbf{q}) S_{n'l_3}(\mathbf{k}) + A^{(3)}_{nn'}(-\mathbf{k}) S^*_{nl_1}(\mathbf{q}) S_{nl_2}(\mathbf{q}-\mathbf{k}) T_{n'l_3}(-\mathbf{k}) + A^{(3)}_{nn'}(-\mathbf{k}) T^*_{nl_1}(-\mathbf{q}) T_{nl_2}(\mathbf{k}-\mathbf{q}) T_{n'l_3}(-\mathbf{k}) + A^{(3)}_{nn'}(-\mathbf{q}) T^*_{n'l_1}(-\mathbf{q}) S_{nl_2}(\mathbf{q}-\mathbf{k}) T_{nl_3}(-\mathbf{k}) + A^{(3)}_{nn'}(\mathbf{q}) S^*_{n'l_1}(\mathbf{q}) T_{nl_2}(\mathbf{k}-\mathbf{q}) S_{nl_3}(\mathbf{k}) \Big\}, \tag{B2}$$

$$V_3(\mathbf{k},\mathbf{q}|l_1,l_2,l_3) = \sum_{nn'} \Big\{ A^{(3)}_{nn'}(\mathbf{k}) S^*_{n'l_1}(\mathbf{k}) S^*_{nl_2}(\mathbf{q}-\mathbf{k}) T^*_{nl_3}(\mathbf{q}) + A^{(3)}_{nn'}(-\mathbf{k}) T^*_{n'l_1}(-\mathbf{k}) T^*_{nl_2}(\mathbf{k}-\mathbf{q}) S^*_{nl_3}(-\mathbf{q}) \Big\}, \tag{B3}$$

$$V_4(\mathbf{k},\mathbf{q}|l_1,l_2,l_3) = \sum_{nn'} \Big\{ A^{(3)}_{nn'}(\mathbf{k}) T_{nl_1}(\mathbf{q}) S_{nl_2}(\mathbf{q}-\mathbf{k}) S_{n'l_3}(\mathbf{k}) + A^{(3)}_{nn'}(-\mathbf{k}) S_{nl_1}(-\mathbf{q}) T_{nl_2}(\mathbf{k}-\mathbf{q}) T_{n'l_3}(-\mathbf{k}) \Big\}. \tag{B4}$$

In terms of the above quantities in Eqs. (35), (37) and (38), we can now define the weighting factors W_i $(i = a, b, c, d, e)$ as

$$W_a = \left[V_1\left(0,\mathbf{q}'|l'',l',l'\right) + V_1\left(\mathbf{q}',\mathbf{q}'|l',l'',l'\right)\right]\left[V_2\left(0,\mathbf{q}|l,l,l''\right) + V_2\left(\mathbf{q},\mathbf{q}|l,l'',l\right)\right], \tag{B5}$$

$$W_b = \left[V_2\left(0,\mathbf{q}'|l'',l',l'\right) + V_2\left(\mathbf{q}',\mathbf{q}'|l',l'',l'\right)\right]\left[V_1\left(0,\mathbf{q}|l,l,l''\right) + V_1\left(\mathbf{q},\mathbf{q}|l,l'',l\right)\right], \tag{B6}$$

$$W_d = \left[V_1\left(\mathbf{q}',\mathbf{q}|l',l'',l\right) + V_1\left(\mathbf{q}-\mathbf{q}',\mathbf{q}|l'',l',l\right)\right] \times \left[V_2\left(\mathbf{q}',\mathbf{q}|l',l'',l\right) + V_2\left(\mathbf{q}-\mathbf{q}',\mathbf{q}|l'',l',l\right)\right], \tag{B7}$$

$$W_e = \left[V_1\left(\mathbf{q}',\mathbf{q}+\mathbf{q}'|l',l,l''\right) + V_1\left(\mathbf{q},\mathbf{q}+\mathbf{q}'|l,l',l''\right)\right] \times \left[V_2\left(\mathbf{q}',\mathbf{q}+\mathbf{q}'|l'',l,l'\right) + V_2\left(\mathbf{q},\mathbf{q}+\mathbf{q}'|l'',l',l\right)\right], \tag{B8}$$

and finally $W_c \equiv w_1 w_2 + w_2 W_{c2} + w_1 W_{c3} + 2W_{c4}$, where

$$w_1 = V_3\left(\mathbf{q}',-\mathbf{q}|l',l'',l\right) + V_3\left(-\mathbf{q}-\mathbf{q}',-\mathbf{q}|l'',l',l\right), \tag{B9}$$

$$w_2 = V_4\left(\mathbf{q}', -\mathbf{q}|l, l'', l'\right) + V_4\left(-\mathbf{q}-\mathbf{q}', -\mathbf{q}|l, l', l''\right), \tag{B10}$$

$$\begin{aligned} W_{c2} = {} & V_3\left(\mathbf{q}, -\mathbf{q}'|l, l'', l'\right) + V_3\left(-\mathbf{q}-\mathbf{q}', -\mathbf{q}'|l'', l, l'\right) \\ & + V_3\left(\mathbf{q}, \mathbf{q}+\mathbf{q}'|l, l', l''\right) + V_3\left(\mathbf{q}', \mathbf{q}+\mathbf{q}'|l', l, l''\right), \end{aligned} \tag{B11}$$

$$\begin{aligned} W_{c3} = {} & V_4\left(\mathbf{q}, -\mathbf{q}'|l', l'', l\right) + V_4\left(-\mathbf{q}-\mathbf{q}', -\mathbf{q}'|l', l, l''\right) \\ & + V_4\left(\mathbf{q}, \mathbf{q}+\mathbf{q}'|l'', l', l\right) + V_4\left(\mathbf{q}', \mathbf{q}+\mathbf{q}'|l'', l, l'\right), \end{aligned} \tag{B12}$$

$$\begin{aligned} W_{c4} = {} & \left[V_3\left(\mathbf{q}', -\mathbf{q}|l', l'', l\right) + V_3\left(-\mathbf{q}-\mathbf{q}', -\mathbf{q}|l'', l', l\right) + \right. \\ & \left. V_3\left(\mathbf{q}', \mathbf{q}+\mathbf{q}|l', l, l''\right) + V_3\left(\mathbf{q}, \mathbf{q}+\mathbf{q}'|l, l', l''\right)\right] \\ & \times \left[V_4\left(\mathbf{q}', -\mathbf{q}|l, l'', l'\right) + V_4\left(-\mathbf{q}-\mathbf{q}', -\mathbf{q}'|l, l', l''\right) + \right. \\ & \left. V_4\left(\mathbf{q}', \mathbf{q}+\mathbf{q}'|l'', l, l'\right) + V_4\left(\mathbf{q}, \mathbf{q}+\mathbf{q}'|l'', l', l\right)\right]. \end{aligned} \tag{B13}$$

APPENDIX C: FOUR-MAGNON AMPLITUDE FACTORS

The expressions for the amplitude factor Λ_i $(i = 1, 2, 3)$ in Eq. (39), and hence for the vertices in the diagrams in Fig. 6, are given by

$$\begin{aligned} \Lambda_1(\mathbf{k}\mathbf{k}'\mathbf{q}|l_1 l_2 l_3 l_4) = {} & \sum_{nn'} \Big\{ A^{(4)}_{nn'}(\mathbf{k}) \Big[S^*_{n,l_1}(\mathbf{k}') S^*_{n,l_2}(\mathbf{q}-\mathbf{k}') S_{n,l_3}(\mathbf{q}-\mathbf{k}) S_{n',l_4}(\mathbf{k}) + 2 S^*_{n,l_1}(\mathbf{k}') \times \\ & T^*_{n,l_2}(\mathbf{k}'-\mathbf{q}) T_{n,l_3}(\mathbf{k}-\mathbf{q}) S_{n',l_4}(\mathbf{k}) + T^*_{n,l_1}(-\mathbf{k}') T^*_{n,l_2}(\mathbf{k}-\mathbf{q}) T_{n,l_3}(\mathbf{k}'-\mathbf{q}) \times \\ & T_{n',l_4}(-\mathbf{k}) + 2 T^*_{n,l_1}(-\mathbf{k}') S^*_{n,l_2}(\mathbf{q}-\mathbf{k}') S_{n,l_3}(\mathbf{q}-\mathbf{k}) T_{n',l_4}(-\mathbf{k}) \Big] + A^{(4)}_{n,n'}(\mathbf{k}') \times \\ & \Big[T^*_{n',l_1}(-\mathbf{k}') T^*_{n,l_2}(\mathbf{k}-\mathbf{q}) T_{n,l_3}(\mathbf{k}'-\mathbf{q}) T_{n,l_4}(-\mathbf{k}) + 2 T^*_{n',l_1}(-\mathbf{k}') \times \\ & S^*_{n,l_2}(\mathbf{q}-\mathbf{k}') S_{n,l_3}(\mathbf{q}-\mathbf{k}) T_{n,l_4}(-\mathbf{k}) + S^*_{n',l_1}(\mathbf{k}') S^*_{n,l_2}(\mathbf{q}-\mathbf{k}') \times \\ & S_{n,l_3}(\mathbf{q}-\mathbf{k}) S_{n,l_4}(\mathbf{k}) + 2 S^*_{n'',l_1}(\mathbf{k}') T^*_{n,l_2}(\mathbf{k}'-\mathbf{q}) T_{n,l_3}(\mathbf{k}-\mathbf{q}) S_{n,l_4}(\mathbf{k}) \Big] - \\ & 2 A'^{(4)}_{n,n'}(\mathbf{k}-\mathbf{k}') \Big[S^*_{n',l_1}(\mathbf{k}') S^*_{n,l_2}(\mathbf{q}-\mathbf{k}') S_{n,l_3}(\mathbf{q}-\mathbf{k}) S_{n',l_4}(\mathbf{k}) + \\ & T^*_{n',l_1}(-\mathbf{k}') T^*_{n,l_2}(\mathbf{k}-\mathbf{q}) T_{n,l_3}(\mathbf{k}'-\mathbf{q}) T_{n',l_4}(-\mathbf{k}) + S^*_{n',l_1}(\mathbf{k}') T^*_{n,l_2}(\mathbf{k}'-\mathbf{q}) \times \\ & T_{n,l_3}(\mathbf{k}-\mathbf{q}) S_{n',l_4}(\mathbf{k}) + T^*_{n',l_1}(-\mathbf{k}') S^*_{n,l_2}(\mathbf{q}-\mathbf{k}') S_{n,l_3}(\mathbf{q}-\mathbf{k}) T_{n',l_4}(-\mathbf{k}) \Big] - \end{aligned}$$

$$2A'^{(4)}_{n,n'}(\mathbf{q})\left[S^*_{n',l_1}(\mathbf{k}')T^*_{n',l_2}(\mathbf{k}'-\mathbf{q})S_{n,l_3}(\mathbf{q}-\mathbf{k})T_{n,l_4}(-\mathbf{k})+T^*_{n,l_1}(-\mathbf{k}')\times\right.$$
$$\left.S^*_{n,l_2}(\mathbf{q}-\mathbf{k}')T_{n',l_3}(\mathbf{k}-\mathbf{q})S_{n',l_4}(\mathbf{k})\right]+B^{(4)}_{n,n'}(\mathbf{k})\left[T^*_{n,l_1}(-\mathbf{k}')T^*_{n,l_2}(\mathbf{k}'-\mathbf{q})\times\right.$$
$$\left.T_{n,l_3}(\mathbf{k}-\mathbf{q})S_{n',l_4}(\mathbf{k})+2S^*_{n,l_1}(\mathbf{k}')T^*_{n,l_2}(\mathbf{k}'-\mathbf{q})S_{n,l_3}(\mathbf{q}-\mathbf{k})S_{n',l_4}(\mathbf{k})\right]+$$
$$B^{(4)}_{n,n'}(-\mathbf{k}')\left[T^*_{n',l_1}(-\mathbf{k}')S^*_{n,l_2}(\mathbf{q}-\mathbf{k}')S_{n,l_3}(\mathbf{q}-\mathbf{k})S_{n,l_4}(\mathbf{k})+2T^*_{n',l_1}(-\mathbf{k}')\times\right.$$
$$\left.T^*_{n,l_2}(\mathbf{k}'-\mathbf{q})S_{n,l_3}(\mathbf{q}-\mathbf{k})T_{n,l_4}(-\mathbf{k})\right]+C^{(4)}_{n,n'}(\mathbf{k}')\left[S^*_{n',l_1}(\mathbf{k}')T^*_{n,l_2}(\mathbf{k}'-\mathbf{q})\times\right.$$
$$\left.T_{n,l_3}(\mathbf{k}-\mathbf{q})T_{n,l_4}(-\mathbf{k})+2S^*_{n',l_1}(\mathbf{k}')S^*_{n,l_2}(\mathbf{q}-\mathbf{k}')T_{n,l_3}(\mathbf{k}-\mathbf{q})S_{n,l_4}(\mathbf{k})\right]+$$
$$C^{(4)}_{n,n'}(-\mathbf{k})\left[S^*_{n,l_1}(\mathbf{k}')S^*_{n,l_2}(\mathbf{q}-\mathbf{k}')S_{n,l_3}(\mathbf{q}-\mathbf{k})T_{n',l_4}(-\mathbf{k})+\right.$$
$$\left.\left.2S^*_{n,l_1}(\mathbf{k}')T^*_{n,l_2}(\mathbf{k}'-\mathbf{q})T_{n,l_3}(\mathbf{k}-\mathbf{q})T_{n',l_4}(-\mathbf{k})\right]\right\}, \tag{C1}$$

$$\Lambda_2(\mathbf{k}\mathbf{k}'\mathbf{q}|l_1l_2l_3l_4)=\sum_{n,n'}\left\{A^{(4)}_{n,n'}(\mathbf{k})\left[T^*_{n,l_1}(-\mathbf{q})T_{n,l_2}(\mathbf{k}+\mathbf{k}'-\mathbf{q})T_{n,l_3}(-\mathbf{k}')S_{n',l_4}(\mathbf{k})+2S^*_{n,l_1}(\mathbf{q})\times\right.\right.$$
$$T_{n,l_2}(\mathbf{k}+\mathbf{k}'-\mathbf{q})S_{n,l_3}(\mathbf{k}')S_{n',l_4}(\mathbf{k})+S^*_{n,l_1}(\mathbf{q})S_{n,l_2}(\mathbf{q}-\mathbf{k}-\mathbf{k}')S_{n,l_3}(\mathbf{k}')\times$$
$$\left.T_{n',l_4}(-\mathbf{k})+2T^*_{n,l_4}(-\mathbf{q})T_{n,l_2}(\mathbf{k}+\mathbf{k}'-\mathbf{q})S_{n,l_3}(\mathbf{k}')T_{n',l_4}(-\mathbf{k})\right]+A^{(4)}_{n,n'}(\mathbf{q})\times$$
$$\left[T^*_{n',l_1}(-\mathbf{q})T_{n,l_2}(\mathbf{k}+\mathbf{k}'-\mathbf{q})S_{n,l_3}(\mathbf{k}')T_{n,l_4}(-\mathbf{k})+S^*_{n',l_1}(\mathbf{q})T_{n,l_2}(\mathbf{k}+\mathbf{k}'-\mathbf{q})\times\right.$$
$$S_{n,l_3}(\mathbf{k}')S_{n',l_4}(\mathbf{k})]-2A'^{(4)}_{n,n'}(\mathbf{k}-\mathbf{q})\left[S^*_{n',l_1}(\mathbf{q})T_{n,l_2}(\mathbf{k}+\mathbf{k}'-\mathbf{q})S_{n,l_3}(\mathbf{k}')+\right.$$
$$\left.S_{n',l_4}(\mathbf{k})+T^*_{n',l_1}(-\mathbf{q})T_{n,l_2}(\mathbf{k}+\mathbf{k}'-\mathbf{q})S_{n,l_3}(\mathbf{k}')T_{n',l_4}(-\mathbf{k})\right]-$$
$$2A'^{(4)}_{n,n'}(\mathbf{k}+\mathbf{k}')\left[S^*_{n,l_1}(\mathbf{q})S_{n,l_2}(\mathbf{q}-\mathbf{k}-\mathbf{k}')T_{n',l_3}(-\mathbf{k}')S_{n',l_4}(\mathbf{k})+\right.$$
$$\left.T^*_{n,l_1}(-\mathbf{q})T_{n,l_2}(\mathbf{k}+\mathbf{k}'-\mathbf{q})T_{n',l_3}(-\mathbf{k}')S_{n',l_4}(\mathbf{k})\right]+B^{(4)}_{n,n'}(\mathbf{k})\left[S^*_{n,l_1}(\mathbf{q})\times\right.$$
$$S_{n,l_2}(\mathbf{q}-\mathbf{k}-\mathbf{k}')S_{n,l_3}(\mathbf{k}')S_{n',l_4}(\mathbf{k})+2T^*_{n,l_1}(-\mathbf{q})S_{n,l_2}(\mathbf{q}-\mathbf{k}-\mathbf{k}')$$
$$T_{n,l_3}(-\mathbf{k}')S_{n',l_4}(\mathbf{k})]+C^{(4)}_{n,n'}(-\mathbf{k})\left[T^*_{n,l_1}(-\mathbf{q})T_{n,l_2}(\mathbf{k}+\mathbf{k}'-\mathbf{q})\times\right.$$
$$T_{n,l_3}(-\mathbf{k}')T_{n',l_4}(-\mathbf{k})+2S^*_{n,l_1}(\mathbf{q})T_{n,l_2}(\mathbf{k}+\mathbf{k}'-\mathbf{q})S_{n,l_3}(\mathbf{k}')\times$$
$$T_{n',l_4}(-\mathbf{k})]+B^{(4)}_{n,n'}(-\mathbf{q})\left[T^*_{n',l_1}(-\mathbf{q})S_{n,l_2}(\mathbf{q}-\mathbf{k}-\mathbf{k}')S_{n,l_3}(\mathbf{k}')\times\right.$$
$$\left.\left.T_{n,l_4}(-\mathbf{k})]+C^{(4)}_{n,n'}(\mathbf{q})\left[S^*_{n',l_1}(\mathbf{q})T_{n,l_2}\left(\mathbf{k}+\mathbf{k}'-q\right)T_{n,l_3}(-\mathbf{k}')S_{n,l_4}(\mathbf{k})\right]\right\}, \tag{C2}$$

$$\Lambda_3(\mathbf{k}\mathbf{k}'\mathbf{q}|l_1l_2l_3l_4)=\sum_{n,n'}\left\{A^{(4)}_{n,n'}(-\mathbf{k})\left[T^*_{n',l_1}(-\mathbf{k})S^*_{n,l_2}(\mathbf{k}')S^*_{n,l_3}(\mathbf{q}-\mathbf{k}-\mathbf{k}')S_{n,l_4}(\mathbf{q})+\right.\right.$$
$$2T^*_{n',l_1}(-\mathbf{k})S^*_{n,l_2}(\mathbf{k}')T^*_{n,l_3}(\mathbf{k}+\mathbf{k}'-\mathbf{q})T_{n,l_4}(-\mathbf{q})+S^*_{n',l_1}(\mathbf{k})\times$$

$$
\begin{aligned}
&T^*_{n,l_2}(-\mathbf{k}')T^*_{n,l_3}(\mathbf{k}+\mathbf{k}'-\mathbf{q})T_{n,l_4}(-\mathbf{q}) + 2S^*_{n',l_1}(\mathbf{k})S^*_{n,l_2}(\mathbf{k}') \times \\
&T^*_{n,l_3}(\mathbf{k}+\mathbf{k}'-\mathbf{q})S_{n,l_4}(\mathbf{q})\Big] + A^{(4)}_{n,n'}(\mathbf{q})\left[S^*_{n,l_1}(\mathbf{k})S^*_{n,l_2}(\mathbf{k}')\times\right. \\
&T^*_{n,l_3}(\mathbf{k}+\mathbf{k}'-\mathbf{q})S_{n',l_4}(\mathbf{q}) + T^*_{n,l_1}(-\mathbf{k})T^*_{n,l_2}(-\mathbf{k}')S^*_{n,l_3}(\mathbf{q}-\mathbf{k}-\mathbf{k}') \times \\
&T_{n',l_4}(-\mathbf{q})] - 2A'^{(4)}_{n,n'}(\mathbf{k}-\mathbf{q})\left[S^*_{n',l_1}(\mathbf{k})S^*_{n,l_2}(\mathbf{k}')T^*_{n,l_3}(\mathbf{k}+\mathbf{k}'-\mathbf{q})\times\right. \\
&S_{n',l_4}(\mathbf{q}) + T^*_{n',l_1}(-\mathbf{k})T^*_{n,l_2}(-\mathbf{k}')S^*_{n,l_3}(\mathbf{q}-\mathbf{k}-\mathbf{k}')T_{n',l_4}(-\mathbf{q})\Big] - \\
&2A'^{(4)}_{n,n'}(\mathbf{k}+\mathbf{k}')\left[T^*_{n',l_1}(-\mathbf{k})S^*_{n',l_2}(\mathbf{k}')S^*_{n,l_3}(\mathbf{q}-\mathbf{k}-\mathbf{k}')S_{n,l_4}(\mathbf{q})+\right. \\
&T^*_{n',l_1}(-\mathbf{k})S^*_{n',l_2}(\mathbf{k}')T^*_{n,l_3}(\mathbf{k}+\mathbf{k}'-\mathbf{q})T_{n,l_4}(-\mathbf{q})\Big] + B^{(4)}_{n,n'}(-\mathbf{k}) \times \\
&\Big[T^*_{n',l_1}(-\mathbf{k})T^*_{n,l_2}(-\mathbf{k}')T^*_{n,l_3}(\mathbf{k}+\mathbf{k}'-\mathbf{q})T_{n,l_4}(-\mathbf{q}) + 2T^*_{n',l_1}(-\mathbf{k})\times \\
&S^*_{n,l_2}(\mathbf{k}')T^*_{n,l_3}(\mathbf{k}+\mathbf{k}'-\mathbf{q})S_{n,l_4}(\mathbf{q})\Big] + C^{(4)}_{n,n'}(\mathbf{k})\left[S^*_{n',l_1}(\mathbf{k})S^*_{n,l_2}(\mathbf{k}')\times\right. \\
&S^*_{n,l_3}(\mathbf{q}-\mathbf{k}-\mathbf{k}')S_{n,l_4}(\mathbf{q}) + 2S^*_{n',l_1}(\mathbf{k})S^*_{n,l_2}(\mathbf{k}')T^*_{n,l_3}(\mathbf{k}+\mathbf{k}'-\mathbf{q}) \times \\
&T_{n,l_4}(-\mathbf{q})] + B^{(4)}_{n,n''}(\mathbf{q})\left[S^*_{n,l_1}(\mathbf{k})T^*_{n,l_2}(-\mathbf{k}')T^*_{n,l_3}(\mathbf{k}+\mathbf{k}'-\mathbf{q})S_{n',l_4}(\mathbf{q})\right]. \\
&\left.+C^{(4)}_{n,n'}(-\mathbf{q})\left[T^*_{n,l_1}(-\mathbf{k})S^*_{n,l_2}(\mathbf{k}')S^*_{n,l_3}(\mathbf{q}-\mathbf{k}-\mathbf{k}')T_{n',l_4}(-\mathbf{q})\right]\right\}. \qquad \text{(C3)}
\end{aligned}
$$

The terms Λ_4 and Λ_5 are given by similar expressions. They will not be quoted here, since they do not enter into the expressions for the SW energy shift and damping.

We can now define the weighting factors Θ_i $(i = a, b, c, d)$ in Eqs. (40) and (41) as

$$
\begin{aligned}
\Theta_a = &\Lambda_1(\mathbf{q},\mathbf{q},\mathbf{q}+\mathbf{q}'|l,l',l',l) + \Lambda_1(\mathbf{q},\mathbf{q}',\mathbf{q}+\mathbf{q}'|l',l,l',l) \\
&+ \Lambda_1(\mathbf{q}',\mathbf{q},\mathbf{q}+\mathbf{q}'|l,l',l,l') + \Lambda_1(\mathbf{q}',\mathbf{q}',\mathbf{q}+\mathbf{q}',|l',l,l,l'), \qquad \text{(C4)}
\end{aligned}
$$

$$
\begin{aligned}
\Theta_b = &[\Lambda_1(\mathbf{q},\mathbf{q}'',\mathbf{q}'|l''l'''l'l) + \Lambda_1(\mathbf{q},\mathbf{q}'-\mathbf{q}'',\mathbf{q}'|l'''l''l'l)+ \\
&\Lambda_1(\mathbf{q}'-\mathbf{q},\mathbf{q}'',\mathbf{q}'|l''l'''ll') + \Lambda_1(\mathbf{q}'-\mathbf{q},\mathbf{q}'-\mathbf{q}'',\mathbf{q}'|l'''l''ll')] \times \\
&[\Lambda_1(\mathbf{q}'',\mathbf{q},\mathbf{q}'|ll'l'''l'') + \Lambda_1(\mathbf{q}'',\mathbf{q}'-\mathbf{q},\mathbf{q}'|l'll'''l'')+ \\
&\Lambda_1(\mathbf{q}'-\mathbf{q}'',\mathbf{q},\mathbf{q}'|ll'l''l''') + \Lambda_1(\mathbf{q}'-\mathbf{q}'',\mathbf{q}'-\mathbf{q},\mathbf{q}'|l'll''l''')]\,, \qquad \text{(C5)}
\end{aligned}
$$

$$
\begin{aligned}
\Theta_c = &[\Lambda_2(\mathbf{q}-\mathbf{q}',\mathbf{q}'',\mathbf{q}|ll'''l''l') + \Lambda_2(\mathbf{q}-\mathbf{q}',\mathbf{q}'-\mathbf{q}'',\mathbf{q}|ll''l'''l')+ \\
&\Lambda_2(\mathbf{q}'',\mathbf{q}-\mathbf{q}',\mathbf{q}|ll'''l'l'') + \Lambda_2(\mathbf{q}'',\mathbf{q}'-\mathbf{q}'',\mathbf{q}|ll'l'''l'') +
\end{aligned}
$$

$$\Lambda_2(\mathbf{q}'-\mathbf{q}'',\mathbf{q}'',q|ll'l''l''')+\Lambda_2(\mathbf{q}'-\mathbf{q}'',\mathbf{q}-\mathbf{q}',\mathbf{q}|ll''l'l''')]\times$$
$$[\Lambda_3(\mathbf{q}-\mathbf{q}',\mathbf{q}'',\mathbf{q}|l'l''l'''l)+\Lambda_3(\mathbf{q}-\mathbf{q}',\mathbf{q}'-\mathbf{q}'',\mathbf{q}|l'l'''l''l)+$$
$$\Lambda_3(\mathbf{q}'',\mathbf{q}-\mathbf{q}',\mathbf{q}|l''l'l'''l)+\Lambda_3(\mathbf{q}'',\mathbf{q}'-\mathbf{q}'',\mathbf{q}|l''l'''l'l)+$$
$$\Lambda_3(\mathbf{q}'-\mathbf{q}'',\mathbf{q}'',\mathbf{q}|l'''l''l'l)+\Lambda_3(\mathbf{q}'-\mathbf{q}','\,\mathbf{q}-\mathbf{q}',\mathbf{q}|l'''l'l''l)]\,, \tag{C6}$$

$$\Theta_d=[\Lambda_2(\mathbf{q},\mathbf{q}'',\mathbf{q}'+\mathbf{q}''|l'''l'l''l)+\Lambda_2(\mathbf{q},\mathbf{q}'-\mathbf{q},\mathbf{q}'+\mathbf{q}''|l'''l''l'l)+$$
$$\Lambda_2(\mathbf{q}'',\mathbf{q},\mathbf{q}'+\mathbf{q}''|l'''l'll'')+\Lambda_2(\mathbf{q}'',\mathbf{q}'-\mathbf{q},\mathbf{q}'+\mathbf{q}''|l'''ll'l'')+$$
$$\Lambda_2(\mathbf{q}'-\mathbf{q},\mathbf{q},\mathbf{q}'+\mathbf{q}''|l'''l''ll')+\Lambda_2(\mathbf{q}'-\mathbf{q},\mathbf{q}'',\mathbf{q}'+\mathbf{q}''|l'''ll''l')]\times$$
$$[\Lambda_3(\mathbf{q},\mathbf{q}'',\mathbf{q}'+\mathbf{q}''|ll''l'l''')+\Lambda_3(\mathbf{q},\mathbf{q}'-\mathbf{q},\mathbf{q}'+\mathbf{q}''|ll'l''l''')+$$
$$\Lambda_3(\mathbf{q}'',\mathbf{q},\mathbf{q}'+\mathbf{q}''|l''ll'l''')+\Lambda_3(\mathbf{q}'',\mathbf{q}-\mathbf{q},\mathbf{q}'+\mathbf{q}''|l''l'll''')+$$
$$\Lambda_3(\mathbf{q}'-\mathbf{q},\mathbf{q},\mathbf{q}'+\mathbf{q}''|l'll''l''')+\Lambda_3(\mathbf{q}'-\mathbf{q},\mathbf{q}'',\mathbf{q}'+\mathbf{q}''|l'l''ll''')]\,. \tag{C7}$$

REFERENCES

* Electronic address: rai@fisica.ufc.br

[1] See, e.g., J.A.C. Bland and B. Heinrich (eds.), *Ultrathin Magnetic Structures, I and II.* Springer-Verlag. Berlin (1994).

[2] N. D. Mermin and H. Wagner, *Phys. Rev. Lett.* **17**, 1133 (1966).

[3] Y. Yafet, J. Kwo, and E. M. Gyorgy, *Phys. Rev. B***33**, 6519 (1986).

[4] R.W. Damon and J.R. Eshbach, *J. Phys. Chem. Solids* **19**, 308 (1961).

[5] T. Wolfram, and R. E. De Wames, *Progr. Surf. Sci.* **2**, 233 (1972).

[6] P. E. Wigen (ed.), *Nonlinear Phenomena and Chaos in Magnetic Materials.* World Scientific. Singapore (1994).

[7] M. G. Cottam (ed.), *Linear and Nonlinear Spin Waves in Magnetic Films and Superlattices.* World Scientific. Singapore (1994).

[8] H. Benson, and D. L. Mills, *Phys. Rev.* **178**, 839 (1969).

[9] R. P. Erickson, and D. L. Mills, *Phys. Rev. B***43**, 10715 (1991).

[10] R. P. Erickson, and D. L. Mills, *Phys. Rev. B***44**, 11825 (1991).

[11] F. C. Nörtemann, R. L. Stamps, and R. E. Camley, *Phys. Rev. B***47**, 11910 (1993).

[12] F. Keffer, *Handbuch der Physik* **18**, 1 (1966).

[13] V. V. Tarasenko and V. D. Kharitonov, *Sov. Phys. Solid State* **16**, 1031 (1974).

[14] P. Mazur and D. L. Mills, *Phys. Rev. B* **29**, 5081 (1984).

[15] D. Kontos and M. G. Cottam, *J. Phys. C* **19**, 1189 (1986).

[16] D. Kontos and M. G. Cottam, *J. Phys. C* **19**, 1203 (1986).

[17] T. S. Rahman and D. L. Mills, *Phys. Rev. B* **20**, 1173 (1979).

[18] See, e.g., G. Srinivasan and A. N. Slavin (eds.), *High Frequency Processes in Magnetic Materials*. World Scientific. Singapore (1995).

[19] P. Grünberg, in *Light Scattering in Solids V*, (eds.) M. Cardona and G. Güntherodt, pp. 303-335. Springer-Verlag. Berlin (1989).

[20] J. Dutcher, in *Linear and Nonlinear Spin Waves in Magnetic Films and Superlattices*, (ed.) M.G. Cottam, pp. 287-333. World Scientific. Singapore (1994).

[21] M. G. Cottam, *J. Phys. C***5**, 2205 (1972).

[22] R. M. White, M. Sparks, and I. Ortenburger, *Phys. Rev.* **139**, A450 (1965).

[23] See, e.g., G. Rickayzen, *Green's Functions and Condensed Matter*. Academic Press. London (1980).

FIGURES

FIG. 1. The effects of the next-nearest neighbor exchange interactions on the SW spectrum in a 16-layer EuO film: (a) SW frequency against J_2/J_1 for $q_x = 0.001$ (solid curve) and $q_x = 0.04$ (dashed curve); (b) SW frequency against q_x for $J_2/J_1 = 0$ (solid curve), $J_2/J_1 = 0.2$ (dashed curve), and $J_2/J_1 = 0.3$ (dot-dashed curve).

FIG. 2. The linear SW dispertion relation for a 16-layer $GdCl_3$ film with next-nearest neighbor exchange $J_2 = 0.25J_1$ solid lines and $J_2 = 0$ dashed lines.

FIG. 3. Diagrammatic representation of (a) the non-interacting Green function and (b) the possible types of proper self-energy contributions of the system.

FIG. 4. Diagrammatic representation of the Dyson series for the renormalized Green function in terms of the self-energy parts.

FIG. 5. Second order diagrams for the self-energy contributions due to three-magnon processes.

FIG. 6. Self-energy diagrams due to four-magnon processes in (a) first order and (b) second order.

FIG. 7. Three-magnon damping of the lowest SW branch (1) vs reduced wave vector $q_x a/\pi$ for EuO films: (a) Total damping (solid curve) and contributions from some of individual (l', l'') processes: (1,1) dot-dashed curve,(1,2)+(2,1) dashed curve, and (2,2) dotted curve; (b) Total damping for the cases of $N = 8$ (solid curve),$N = 16$ (dotted line) for the lowest branch 1, and for $N = 8$ and branch 2 (dashed curve).

FIG. 8. Three-magnon damping for a $GdCl_3$ film with 8 layers for SW branch 1.

FIG. 9. As in Fig. 8, but for a Fe film.

FIG. 10. Temperature dependence of the three-magnon damping for a 8-layer EuO film with a fixed value of the wave vector ($q_x/\pi = 0.5$), showing (a) splitting processes (solid curve), b) confluence processes (dashed curve).

FIG. 11. SW energy shift vs reduced wave vector $q_x a/\pi$ for EuO films with $N = 8$ (solid curve) and $N = 16$ (dotted curve) for the lowest branch 1, and $N = 8$ for branch 2 (dashed curve).

FIG. 12. The four-magnon SW energy shift of the lowest branch vs reduced wave vector $q_x a/\pi$ for an EuO film with 8 layers.

FIG. 13. Temperature dependence of the SW energy shift compared for three-magnon (solid curve) and four-magnon (dashed curve) processes.

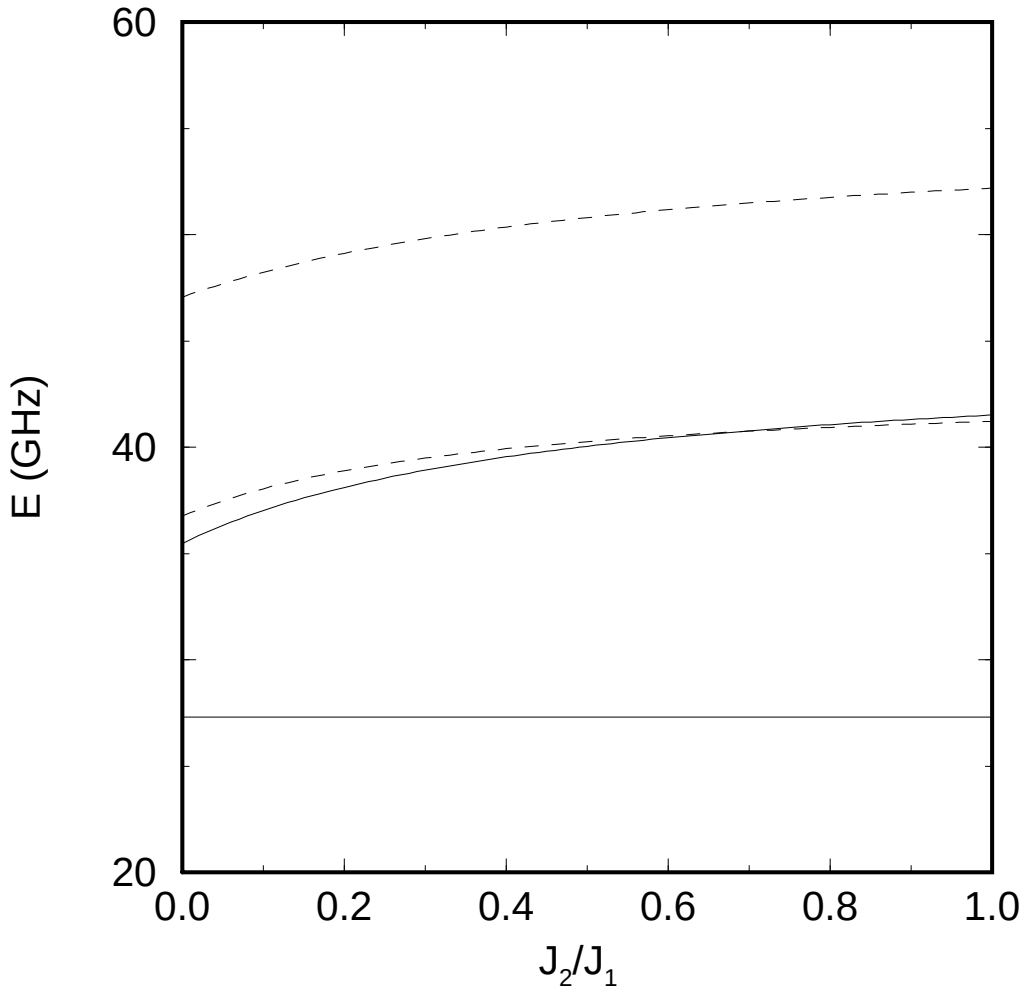

Fig. 1a.

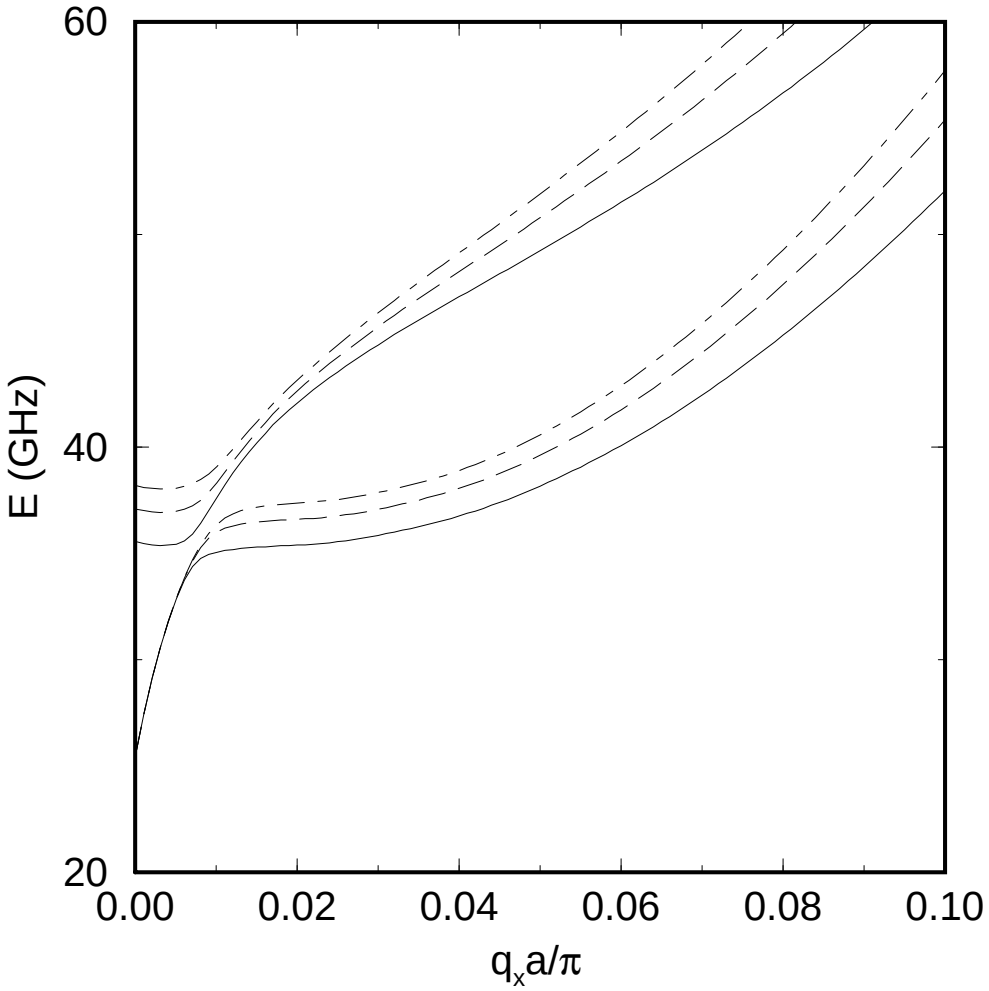

Fig. 1b.

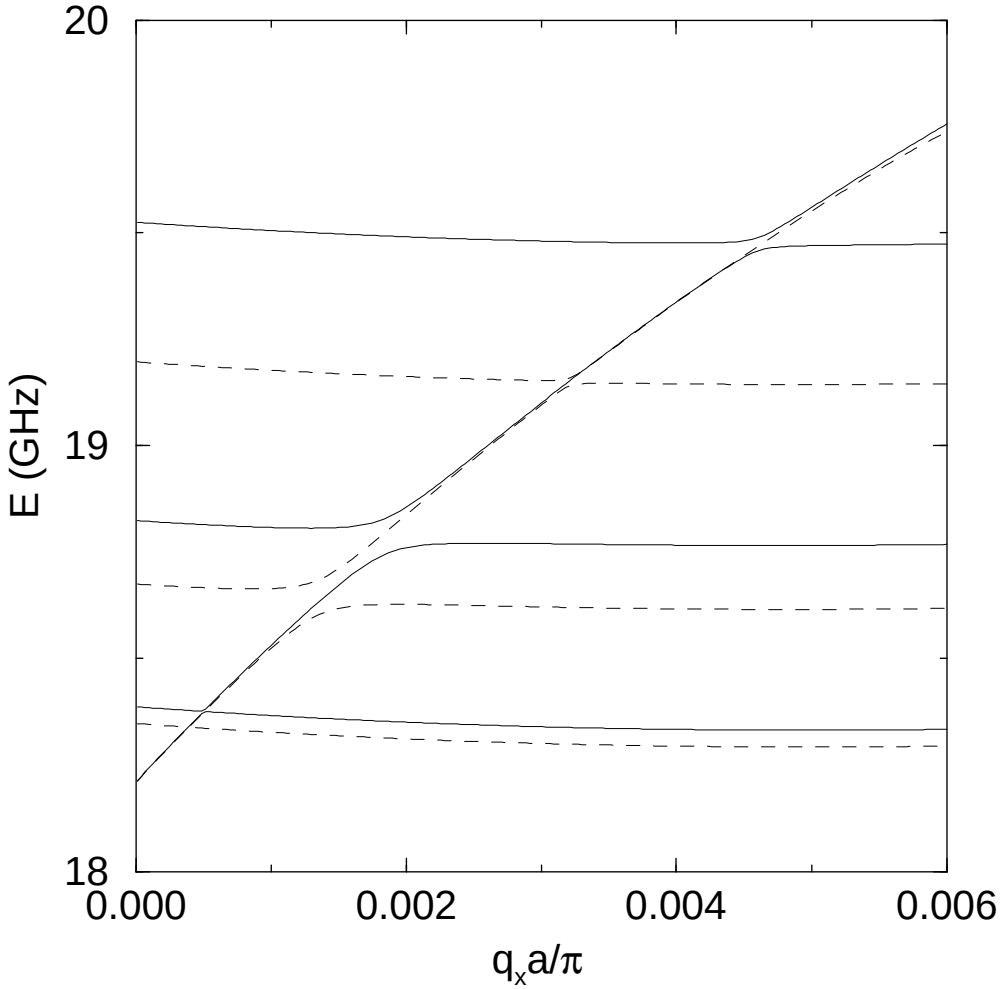

Fig. 2.

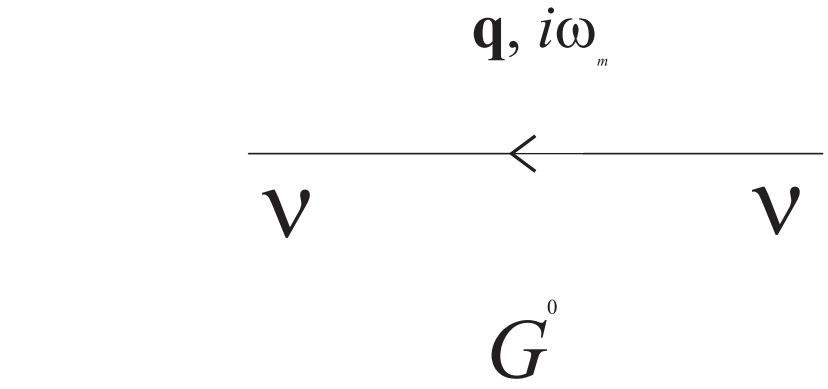

Fig.3a.

Fig. 3b.

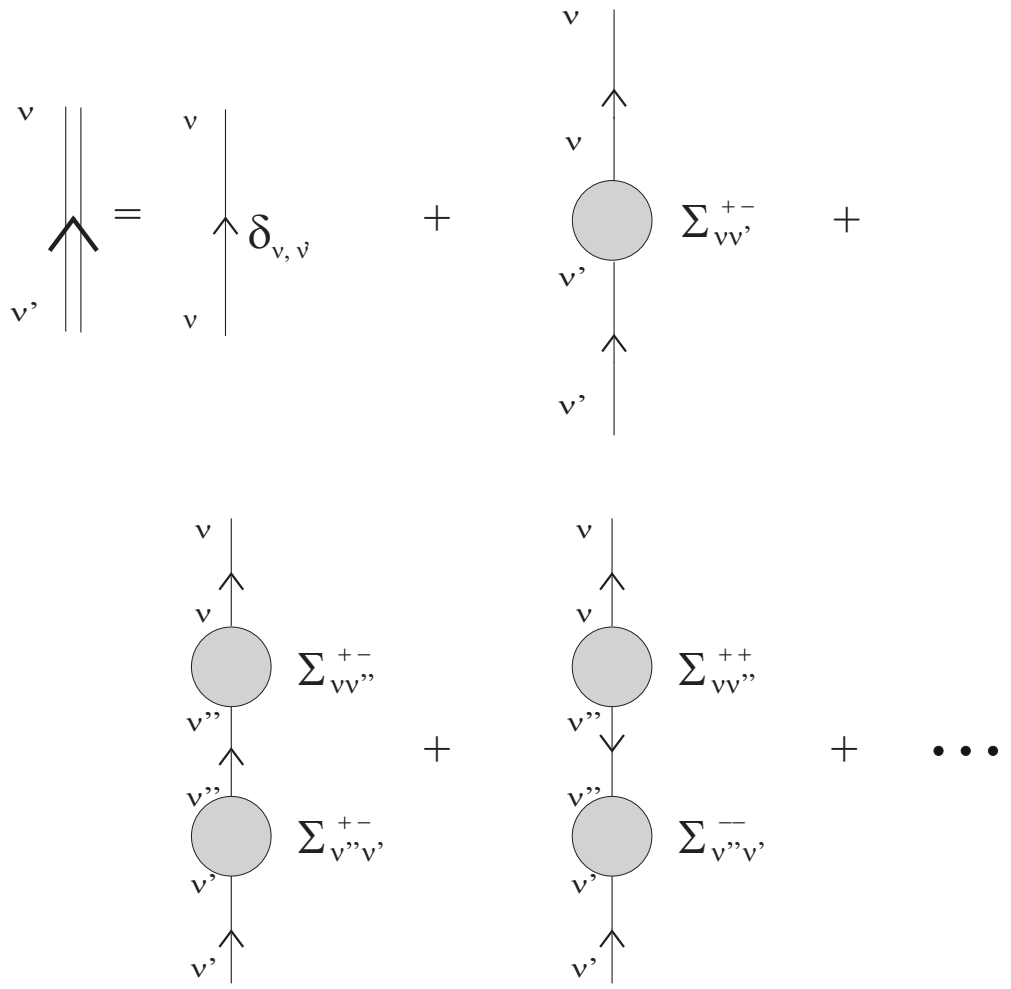

Fig. 4.

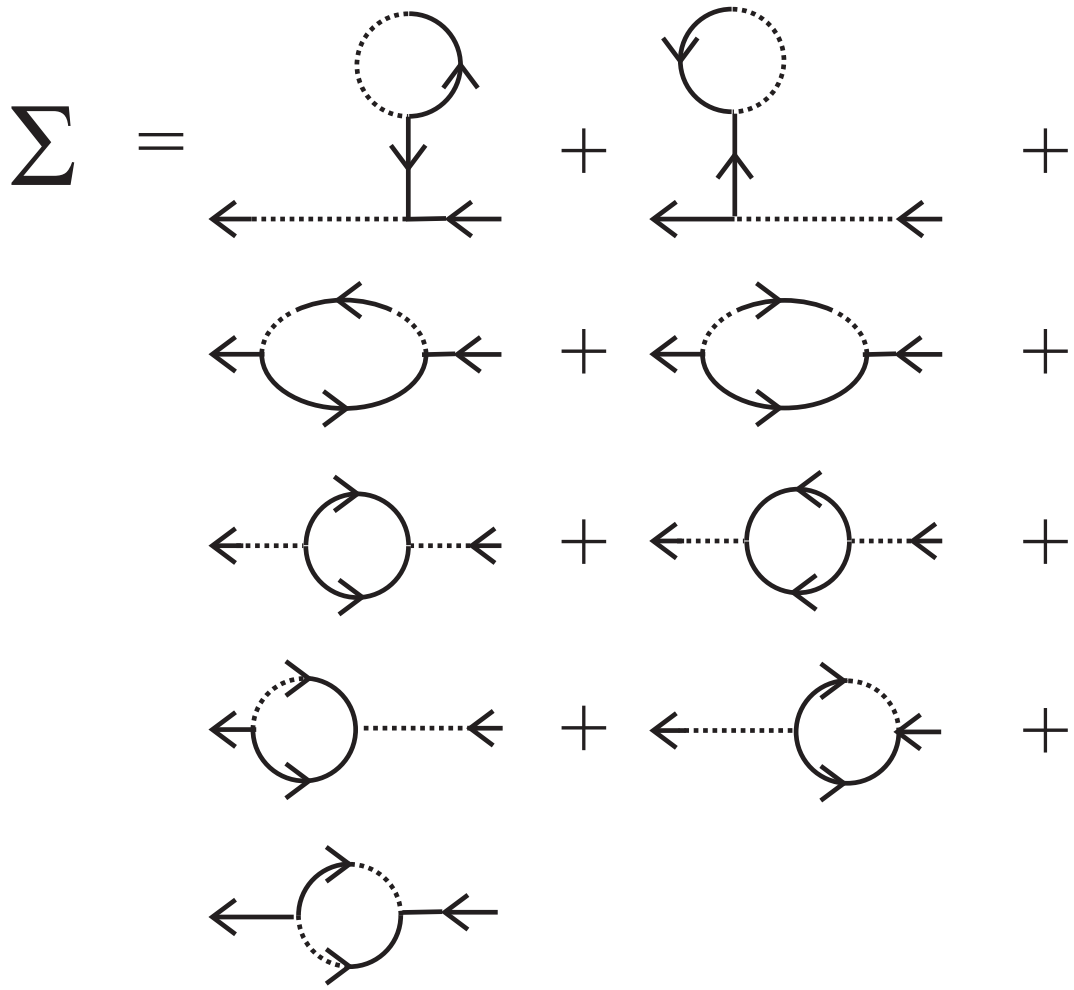

Fig. 5.

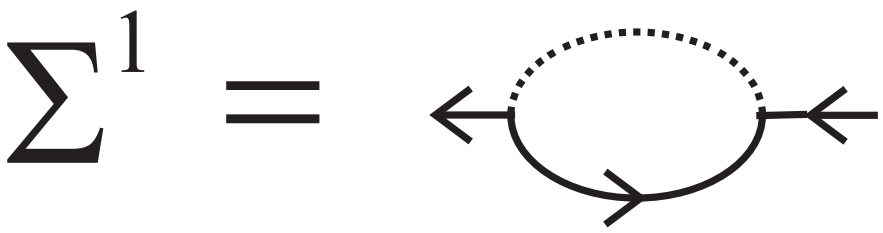

Fig. 6a.

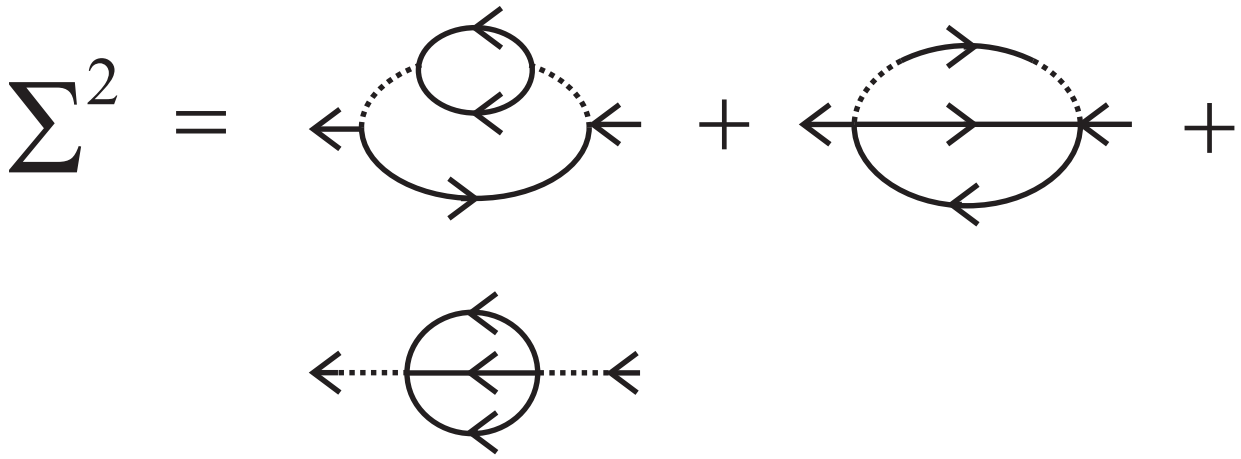

Fig. 6b.

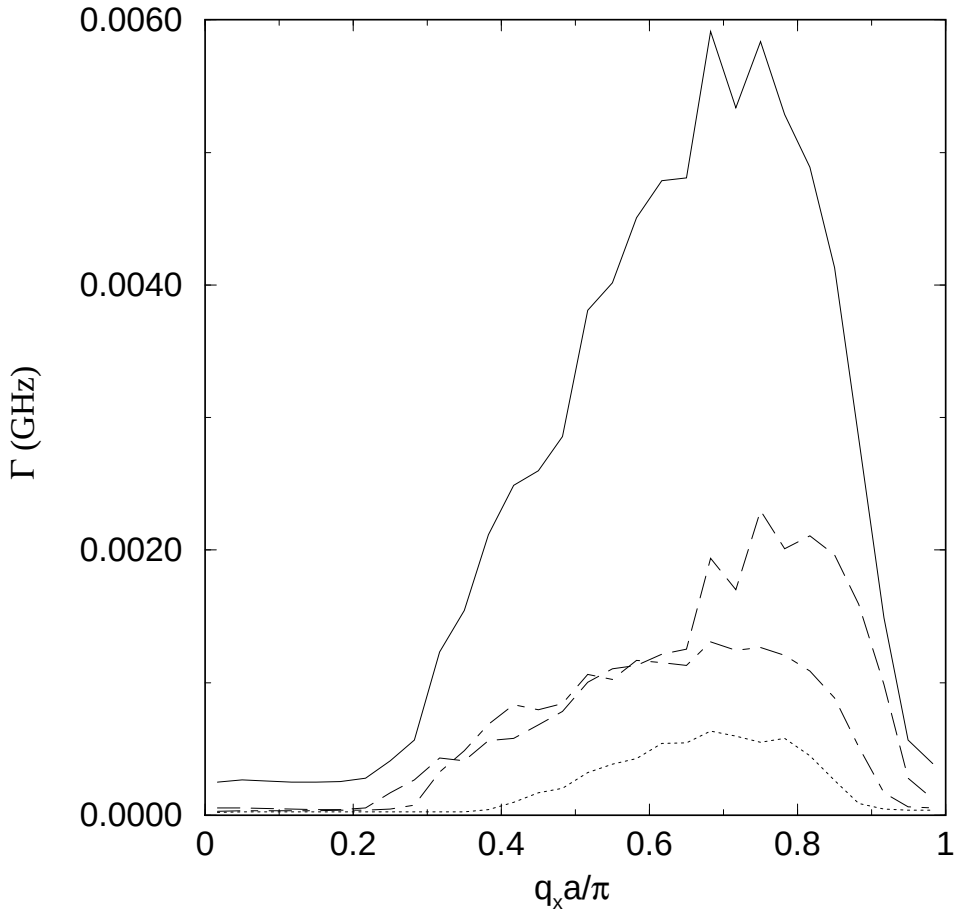

Fig. 7a.

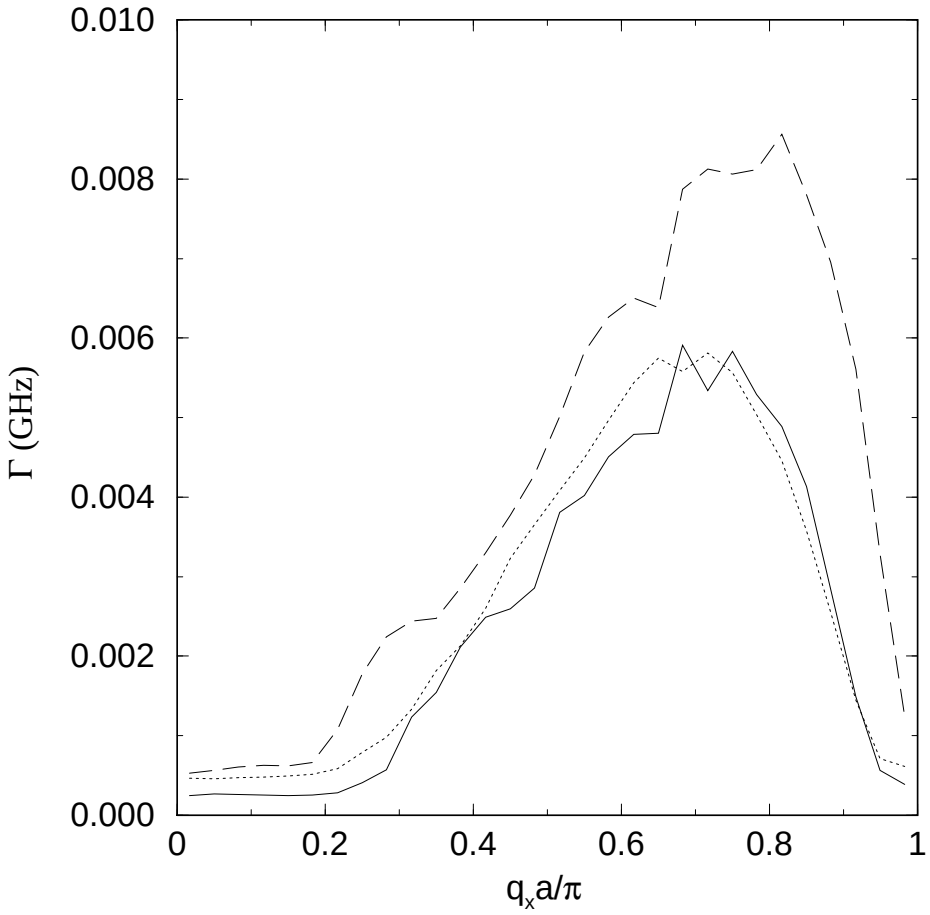

Fig. 7b.

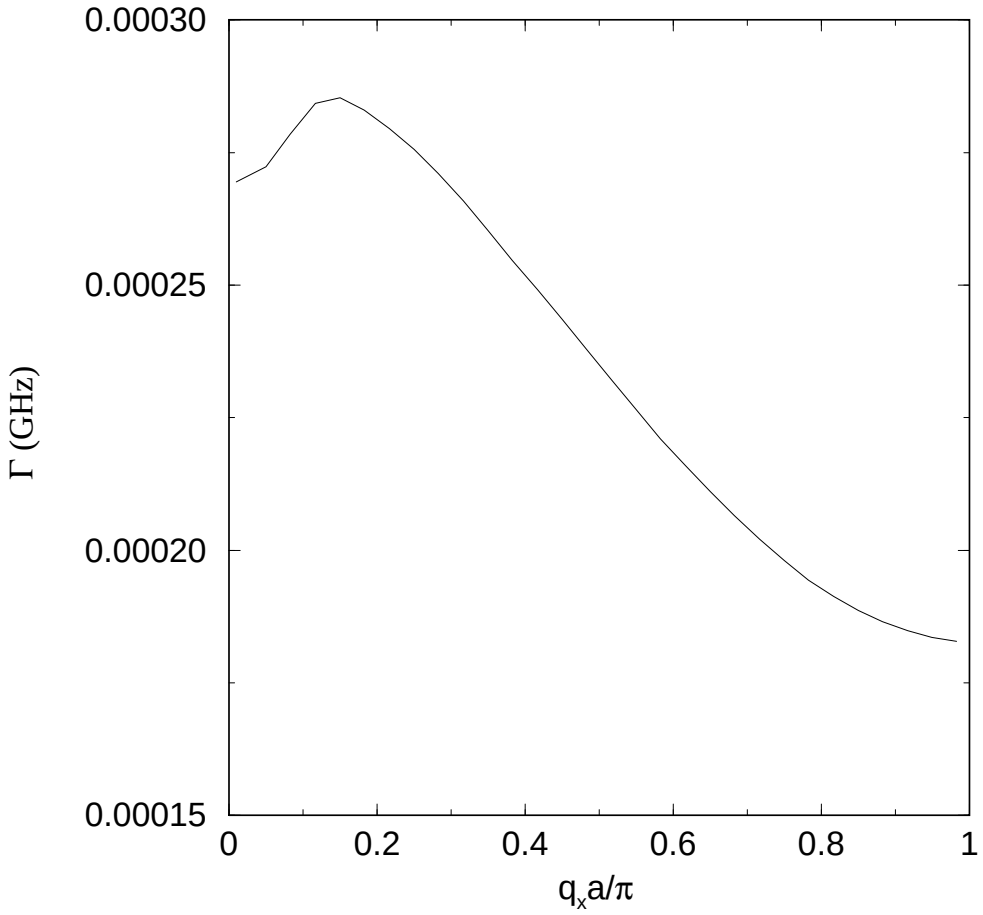

Fig. 8.

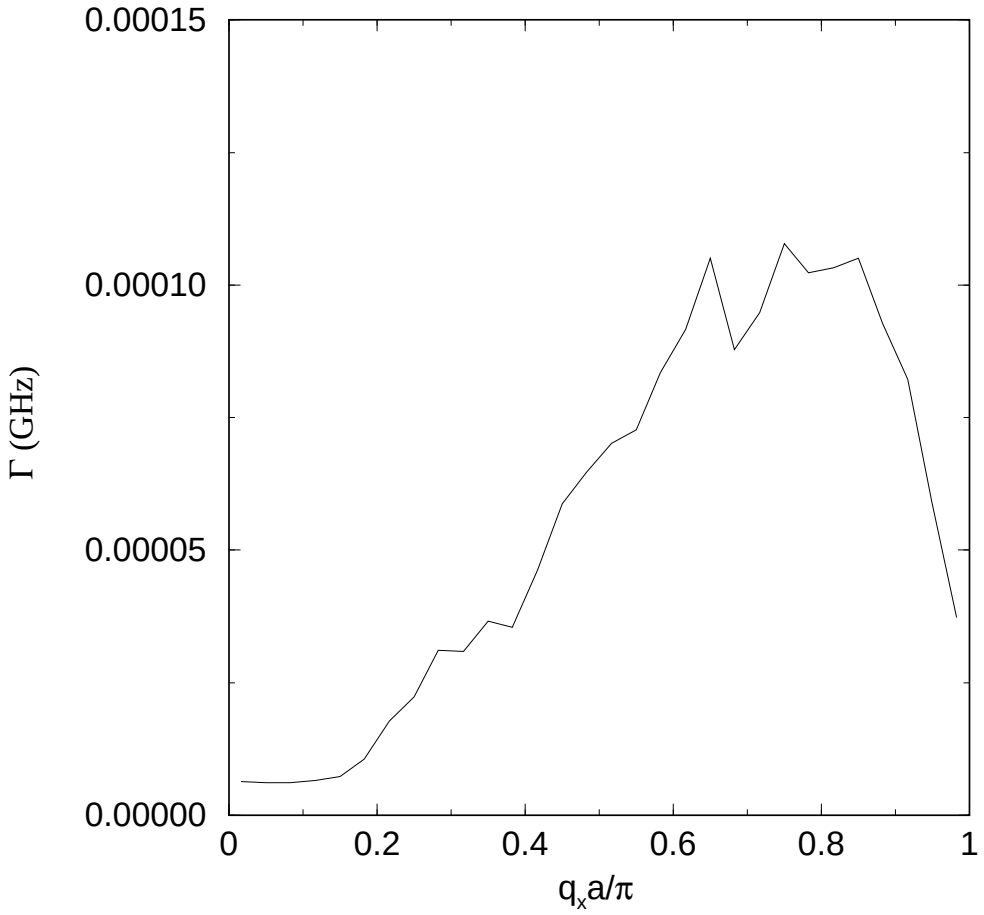

Fig. 9.

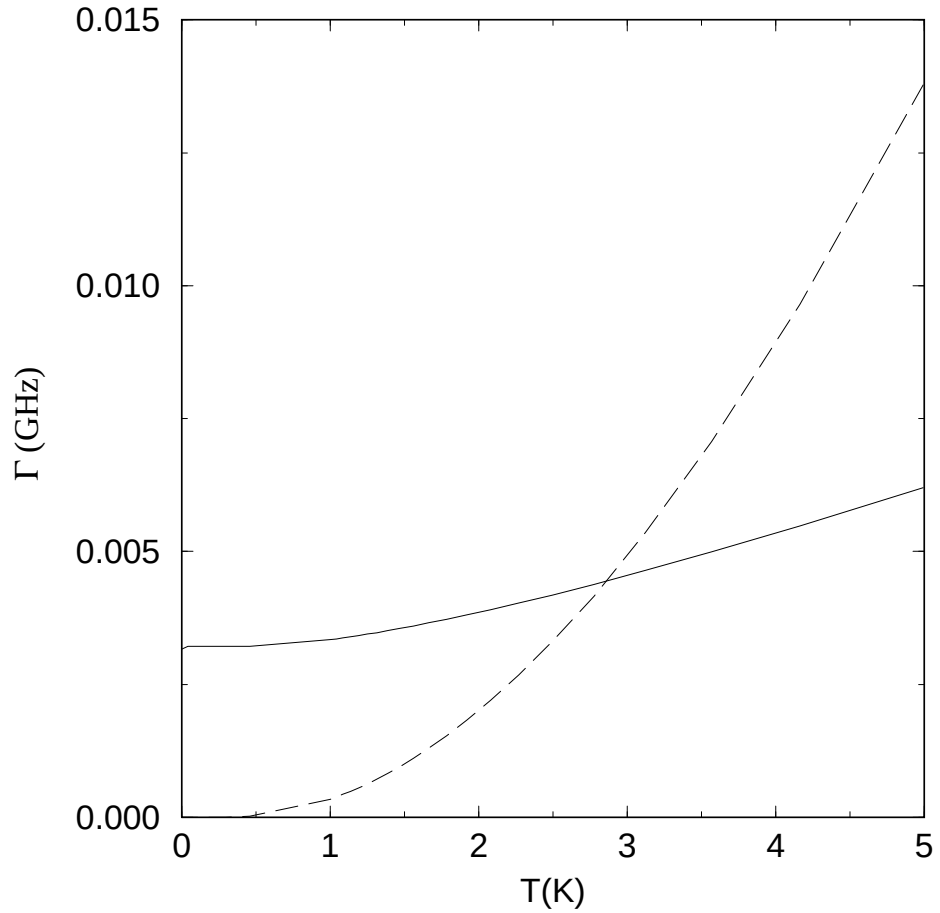

Fig. 10.

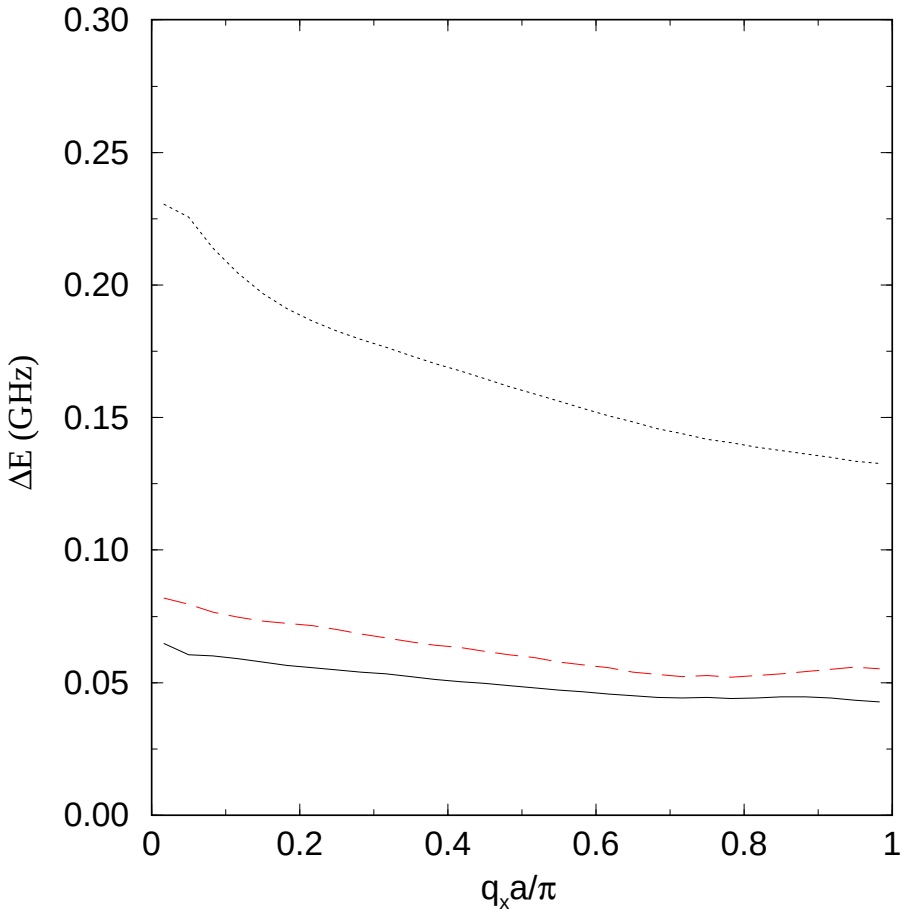

Fig. 11.

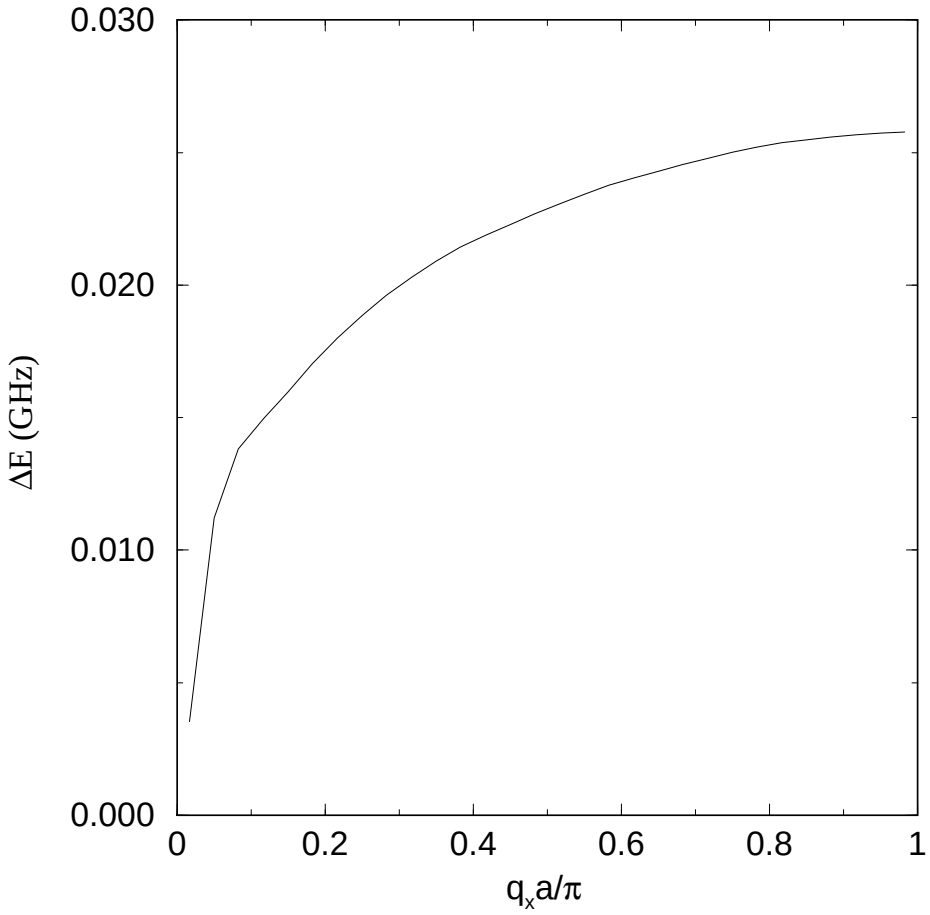

Fig. 12.

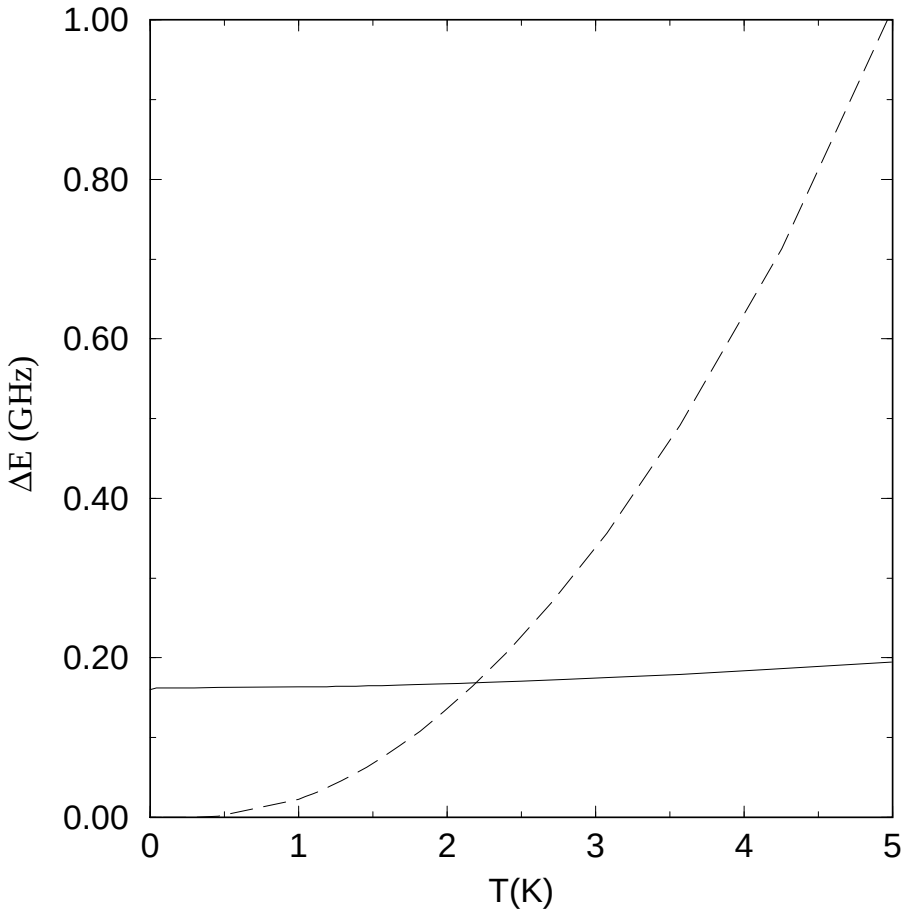

Fig. 13.